AG-336

2. CONVENTIONAL WALL CORRECTIONS FOR CLOSED AND OPEN TEST SECTIONS

Authors : Alex Krynytzky (Chapter 2.1 - 2.3)
Bernd Ewald (Chapter 2.4)

2. CONVENTIONAL WALL CORRECTIONS FOR CLOSED AND OPEN TEST SECTIONS

Investigations of boundary interference in aerodynamic testing date back to the 1920s and 1930s. Glauert's classic monograph on the subject [15] summarises this pioneering work and serves both as a basis for ensuing developments and as a touchstone for evaluating wall interference methods to this day. These early investigations address interference in both closed-wall and open-jet test sections and, to some degree, in test sections whose walls are a combination of these two types. This chapter briefly describes the basic principles of this classical wall interference theory, summarises some fundamental results, and traces several related lines of development since the publication of AGARDograph 109 [13].

The fundamental problem of wall corrections concerns itself with the difference between the flow fields around a body immersed in a uniform oncoming stream of infinite lateral, upstream, and downstream extent, and around the same body in a stream confined or modified by wind tunnel walls. The streamlines around a body in a uniform subsonic onset flow depend on the shape of the body and on the aerodynamic forces acting on the body (which may be considered a result of its shape). In the interference-free case, as distance increases laterally from the body, the streamlines approach the straight and parallel flow of the onset stream. If the wind tunnel's boundaries (the "walls") are far enough away from a model being tested so that the flow perturbation due to the model is negligible, the same uniform parallel flow condition is obtained at the boundary and the flow around the model is therefore not affected by the tunnel boundaries. However, to the extent that the model's influence is perceptible at the boundary, the flow within the tunnel (i.e., around the model) is different from that which would be obtained in an unbounded stream. Classical wall correction theory attempts to account for this difference under a set of simplifying assumptions and corresponding restrictions on the theory's range of applicability. Fundamental to this approach are the concepts of primary corrections and residual variations discussed in Chapter 1.

Elementary interference results for both 2D and 3D models are presented in this chapter. These include the interference of only the tunnel walls remote from the model. So-called sidewall interference, which may be a major source of three-dimensionality in 2D tests, deserves attention as a special interference topic and is beyond the scope of the current discussion. Most of the 3D interference discussion in this chapter addresses a rectangular test section of height, H, and breadth, B, with the test section aspect ratio defined as B/H. Although other test cross sections are in use (e.g., octagonal, circular, elliptical) and interference methods have been developed for these situations, the rectangular section is used as a focus of discussion because of its commonality in practice, and because of the similarity of rectangular section interference to that of other sections of equal area and aspect ratio.

2.1 CLASSICAL WALL CORRECTIONS: BASIC PRINCIPLES, DEFINITIONS, AND ASSUMPTIONS

As used here, the term "classical" refers to the results of the earliest analyses of wind tunnel boundary interference on models in closed-wall and open-jet wind tunnels. The assumptions underlying classical wall interference theory include:

1. Linear potential flow.
2. Perturbation flow at the tunnel boundaries.
3. Model whose dimensions generally are small relative to the tunnel and whose wakes (including both the viscous and vortex wakes) extend straight downstream from the model.
4. Tunnel of constant cross-sectional area extending far upstream and downstream of the model, with boundaries parallel to the direction of the flow far upstream of the model, and whose boundary condition for a given wall is either no flow normal to the wall or a constant pressure at the wall location.

"Conventional" is used as a further classification of wall corrections, which includes the classical. These corrections are based on classical concepts in that the perturbation flow assumptions are used, but model size, wake position, and tunnel boundary conditions are not restricted as above. For present purposes, the tunnel walls are restricted, however, to a fixed geometry with a known pressure-crossflow characteristic. Conventional wall correction methods do not then include specified boundary condition methods or adaptive wall methods. Much of the work reported in AGARDograph 109 [13] satisfies this definition of "conventional", though specified boundary condition methods and adaptive wall methods have appeared in the literature since the 1940s, and are included in AGARDograph 109 [13] as well.

2.1.1 CO-ORDINATE SYSTEM AND GOVERNING EQUATIONS

The co-ordinate system is defined for a conventional wing-body model such that x is the streamwise co-ordinate, y is the lateral or spanwise co-ordinate, and z is the vertical co-ordinate corresponding to the direction of primary lift, Figure 2.1. The origin of the co-ordinate system is typically taken to be on the test section centreline, at the model centre. In 2D flow, the flow field is taken to be invariant with y. Far upstream of the model, the incoming flow is uniform.

Although the definition of classical wall correction methods should properly be restricted to incompressible flows, as mirrored in the early literature, linearised compressibility is included here as a straightforward application of the Goethert transformation (see, for example, Ashley and Landahl, [5]). Thus, the starting point for the development of classical wall interference corrections is the assumption of linearised potential flow between the model and the tunnel boundaries (see Sec. 4.1). Streamline flow is assumed with no allowance for shock waves or separated wakes. The effect of fluid viscosity in the governing equations is ignored. Velocity at any point in the tunnel is the gradient of the potential function in the usual way:

$$\bar{V}(x,y,z) = \nabla\Phi(x,y,z) \tag{2.1}$$

The principle of superposition is a key feature of classical wall interference analysis. This allows the interference flow field to be considered as an incremental flow field to the interference-free flow around

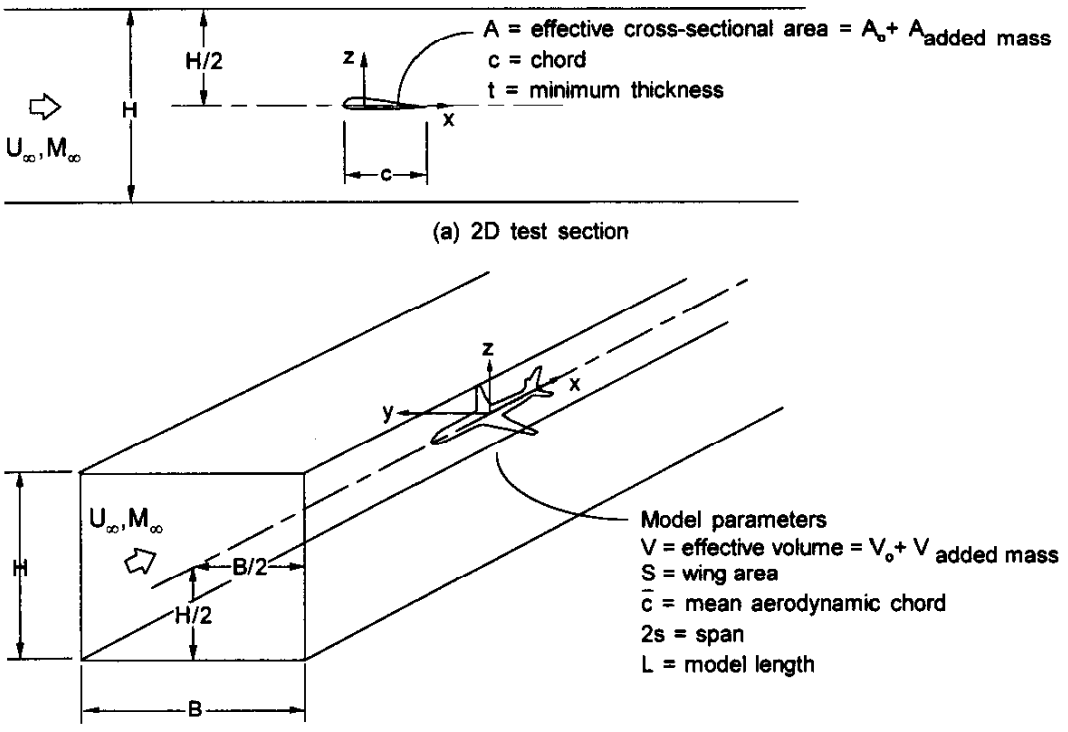

Figure 2.1 : Co-ordinate System and Geometry

the model. Thus, the potential, Φ, is assumed to be expressible as the superposition of a uniform onset stream, the model potential, and the wall potential,

$$\Phi(x,y,z) = -U_\infty x + \varphi_m(x,y,z) + \varphi_w(x,y,z) \tag{2.2}$$

In those regions of the flow away from the model where the flow perturbations to the uniform oncoming stream are small, the model and wall potentials can be considered perturbation velocity potentials. For small deviations from the nominal free stream, the effect of compressibility can be linearised in the full potential equation, resulting in the governing equation for the perturbation velocity potentials,

$$\beta^2 \varphi_{xx} + \varphi_{yy} + \varphi_{zz} = 0 \tag{2.3}$$

where $\beta^2=1-M^2$. That part of the flow field due to the walls, the wall interference velocity field, is the gradient of the wall interference potential,

$$\vec{v}_i(x,y,z) = \frac{\partial \varphi_w}{\partial x}\hat{i} + \frac{\partial \varphi_w}{\partial y}\hat{j} + \frac{\partial \varphi_w}{\partial z}\hat{k} = u_i\hat{i} + v_i\hat{j} + w_i\hat{k} \tag{2.4}$$

The equation for the perturbation velocity potential can be reduced to the Laplace equation ($\nabla^2\varphi=0$) with the co-ordinate transformation (as developed by Prandtl and Glauert for 2D airfoils and extended to three dimensions by Goethert): $X=x$, $Y=\beta y$, and $Z=\beta z$ (see Sec. 4.1). This transformation relates the linearised compressible flow to an equivalent incompressible flow in stretched co-ordinates.

2.1.2 MODEL REPRESENTATION

The combination of perturbation interference flow at the model and small model size (relative to the tunnel) implies that the variation of the interference velocity throughout the volume proximate to the model is small, so that the interference velocity may be considered a constant throughout the region affecting model aerodynamics. The primary corrections to stream magnitude and direction capture the greater part of the wall influence. The next order of corrections considers the linear streamwise variation of interference velocities (which result in streamwise buoyancy and flow curvature corrections). The interference velocities and gradients are typically evaluated at the model centre which, for simple model representations, is the location of singularities that approximate the flow field far from the model.

Thus, the flow in the immediate vicinity of the model will appear as though the model is immersed in an unbounded uniform onset stream of perturbed magnitude and direction relative to the flow far upstream of the model,

$$\vec{V}_{corrected} = U_\infty \hat{i} + \vec{v}_i(0,0,0) = \left(U_\infty + u_i\right)\hat{i} + v_i \hat{j} + w_i \hat{k} \tag{2.5}$$

This corrected onset velocity is characterised by streamwise and upwash velocity corrections (u_i and w_i), commonly referred to as blockage and upwash interference, respectively. For small models it is sufficient to evaluate the interference velocity and its spatial gradients at the model location. For symmetric models at zero yaw, sidewash interference at the plane of symmetry is identically zero.

The magnitude of the streamwise gradient of u_i ($\partial u_i/\partial x$) is a measure of the convergence (or divergence) of the effective onset stream, resulting in a streamwise buoyancy force on the model. The streamwise gradient of w_i ($\partial w_i/\partial x$) is a measure of the curvature of the effective onset stream, resulting in an additional apparent angle of attack (or equivalently, excess lift at a given angle of attack) and pitching moment.

The restriction on wakes extending straight downstream is in no way fundamental, but simply allows the use of simple, analytic solutions to the Prandtl-Glauert equation to represent the model aerodynamics: line doublet (or horseshoe vortex) for 3D lift and its vortex wake, and a point source for drag (2D and 3D viscous wakes).

The assumptions of a small model and of perturbation velocities at the tunnel boundary mean that only the far-field flow around the model must be properly represented. That is, the details of the model are not important; only the integrated effects at the tunnel boundary of model geometry and loading are important to first order.

The first-order far-field influence of the model arises from three independent features of a model's aerodynamics:

1. Model shape and volume, which causes a displacement or bulging of streamlines around the model, with the streamlines reconverging to unperturbated parallel flow downstream of the model.
2. Model lift, which in three dimensions results in a redirection of momentum of the stream, resulting in a downwash field that persists to downstream infinity.
3. Model parasite drag (i.e., not including induced drag or drag due to separated wakes), which results in an outward displacement of streamlines around the viscous wake that also persists downstream of the model.

For small models, these three characteristics are represented by elementary analytical singularities placed at the model location. The requisite singularities derive from potential flow theory and are summarised in Figure 2.2 : line (or in 2D flow, point) vortex to represent lift, source doublet to represent model volume, and point source to represent the displacement effect of the wake. The far field of virtually any flight vehicle of interest can be represented by an appropriate superposition of these singularities at the model location. The effects of finite model extent may be investigated using multiple singularities of these types, though the main features of model size are illustrated by the finite-span horseshoe vortex for wing span and a source-sink combination for body length. Expressions for the potentials of these singularities are given in subsequent sections.

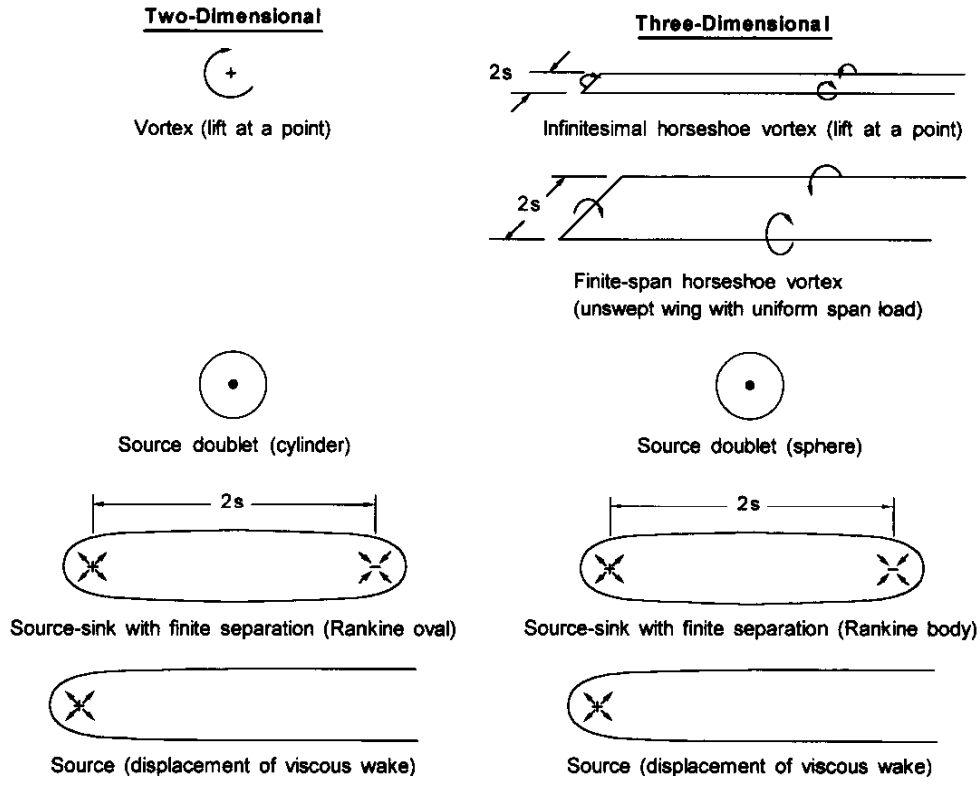

Figure 2.2 Elementary Singularities Used for Model Representation in a Uniform Stream

With the interference velocities at the model location being small, resulting model loading changes (relative to the interference-free case at corrected freestream conditions) are likewise small. This permits the use of singularity strengths taken to be the same as for the interference-free model flow, that is, φ_m is known or specified. For example, a 3D source doublet in a uniform onset flow produces a closed spherical stream surface; thus it represents the potential flow around a sphere. For a sphere in a constrained flow, as in a wind tunnel, this same singularity will produce the same closed spherical stream surface only in the limit of zero model size. Otherwise, the wall potential perturbs the effective closed surface around the doublet; the larger the model size, the greater the deviation. Similarly, use of a specified wing lift distribution (represented by a spanwise distribution of horseshoe vortices) will not fully capture the effect of wall interference on wing loading unless an iterated solution is sought. If model loading changes are not small, due to either model size or sensitivity of the flow to small changes in stream velocity or angle (as at transonic speeds or near stall), classical methods can provide only qualitative guidance, and advanced methods should be considered.

The interference velocities are usually nondimensionalised by the velocity magnitude far upstream of the model,

$$\varepsilon = \frac{u_i}{U_\infty} \tag{2.6}$$

$$\Delta\alpha = \frac{w_i}{U_\infty} \tag{2.7}$$

It is convenient to define an upwash interference parameter (δ) and its streamwise gradient (δ_1),

$$\delta = \frac{w_i}{U_\infty}\frac{C}{SC_L} \tag{2.8}$$

$$\delta_1 = \frac{\partial\delta}{\partial(\frac{x}{\beta L})} \tag{2.9}$$

where C is the test section cross-sectional area, and L is a typical length scale (often taken as the height of the test section).

Similarly, the streamwise gradient of blockage interference is of interest because it affects model forces in addition to the change in the effective freestream velocity given by ε. This gradient imposes a streamwise pressure force, or buoyancy drag, on the model that would not be present in the interference-free flow and that must be subtracted from the measured model drag in the tunnel.

As long as there is a region between the tunnel boundaries and the model satisfying the perturbation flow equations described above, the flow at the tunnel boundaries due to only the model is a perturbation flow, even though the model representation may result in large velocity changes (relative to the free stream) close to the model. Conversely, the flow at the model location due to only the walls will likewise be a perturbation flow, even though the flow close to the walls may be subject to large deviations relative to the oncoming free stream, as in the case of flow through longitudinal slots or in the vicinity of holes. If the wall boundary condition is spatially homogeneous, however, the flow at the wall will satisfy Equation 2.2. This is the case for the closed-wall and idealised open-jet test sections.

It should be noted that even for apparently large models, small model results can provide estimates of the adequacy of applying only primary corrections, based on the magnitude of spatial variations of the interference flow field at the location of the model. Such estimates can then guide the decision on the need for more accurate flow modelling.

2.1.3 TUNNEL WALLS

The condition of tunnel walls extending far upstream and downstream (doubly infinite in streamwise extent) permits the application of the method of images with its corresponding set of analytic results. The method of images is a simple yet powerful technique for the evaluation of interference in tunnels with either closed-wall or open-jet boundaries.

The boundary condition for a closed wall is no flow normal to the wall, given exactly in terms of the perturbation potential,

$$\frac{\partial\varphi}{\partial n} = 0 \tag{2.10}$$

where $\varphi = \varphi_m + \varphi_w$.

Allowing the velocity at the tunnel boundaries to differ from the onset stream velocity by only a small amount (the perturbation velocity) also means that these boundary conditions can be linearised if necessary. The boundary condition for an open wall (or free jet) is a constant pressure equal to the static pressure far upstream of the model; in linearised form,

$$\frac{\partial \varphi}{\partial x} = 0 \tag{2.11}$$

Finally, the assumption of a tunnel of constant cross section (and constant homogeneous boundary conditions for a given wall) extending to infinity both upstream and downstream of the model provides the simplifications (symmetries and asymptotic boundary conditions) permitting the application of analytic techniques, such as the method of images. Because most wind tunnel tests involve a model located on the centreline of the test section, this symmetry condition can be used to advantage both to simplify the analysis and to permit a convenient decoupling of upwash interference from model volume and wake characteristics, and of blockage interference from model lift.

Consider, for example, a planar closed wall extending to infinity in all directions in proximity to an isolated point singularity whose velocity potential is given by $\varphi(x, y, z)$. Figure 2.3 illustrates this situation in two dimensions for the point vortex and source singularities. The desired boundary condition at the wall is $\partial\varphi/\partial n = 0$. If the velocity potential of the singularity is such that $\partial\varphi/\partial n$ is an odd function of the co-ordinate n normal to the wall (i.e., φ is even with respect to n), then by symmetry, the velocity normal to the wall due to this singularity is identically cancelled by placing a so-called image singularity of the same magnitude and strength on the other side of the wall, at the same distance from the wall, on the line normal to the wall and passing through the original singularity. Conversely, if $\partial\varphi/\partial n$ for the original singularity is an even function of the co-ordinate n (i.e., φ is odd with respect to n), the normal velocity at the wall due to the original singularity is cancelled by an image singularity of equal magnitude and opposite strength. Thus for a planar closed wall, the 2D point vortex requires an image of the opposite sense, while a point source requires an image of the same sense.

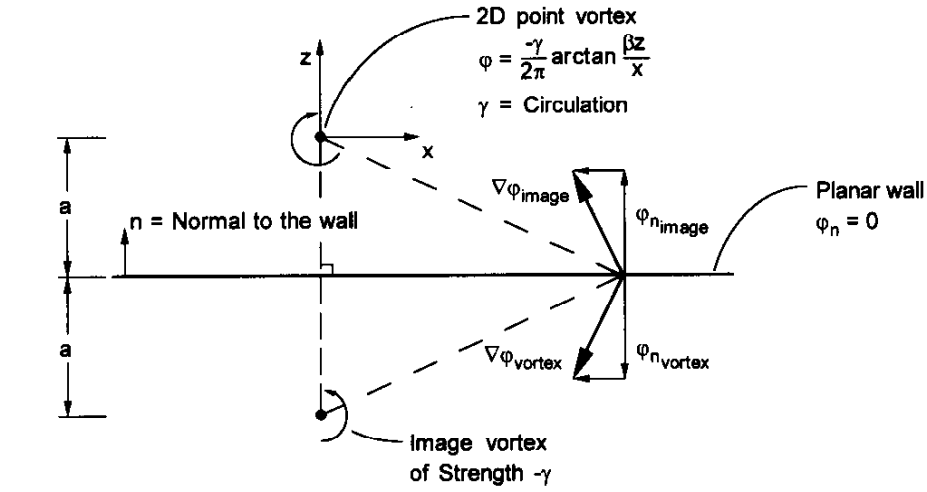

(a) 2D Point Vortex (Model Potential Odd in n)

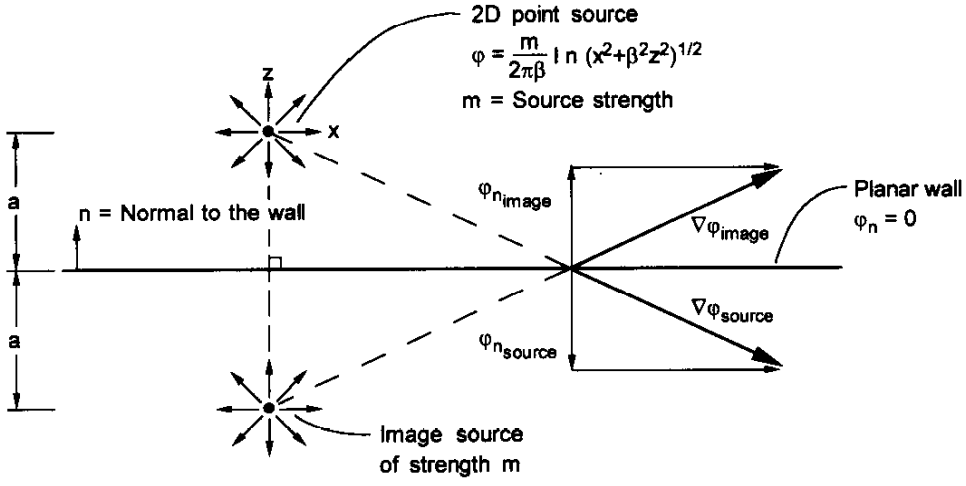

(b) 2D Point Source (Model Potential Even in n)

Figure 2.3 Method of Images for a Planar Closed Wall

Similarly, replacing the planar closed wall by a planar free-jet boundary requires satisfying the linearised constant pressure boundary condition. For the streamwise co-ordinate x parallel to the boundary, if $\partial\varphi/\partial x$ of the original singularity is odd in x, then the image singularity must be of the same magnitude and opposite strength. Conversely, if $\partial\varphi/\partial x$ of the original singularity is an even function of x, then the image singularity must be of equal magnitude and strength. Figure 2.4 illustrates the method of images for a planar free-jet boundary.

It is readily apparent that the method of images is not limited to single point singularities, but can be used for any collection of singularities. Nor is it limited to planar wall boundaries; conformal transformations have been used to develop image systems for octagonal and elliptical tunnels as reported in AGARDograph 109 [13]. The objective is merely to cancel a component of velocity (either normal or streamwise) due to the model at the specified boundary by an appropriate choice of image(s) on the other side of the boundary.

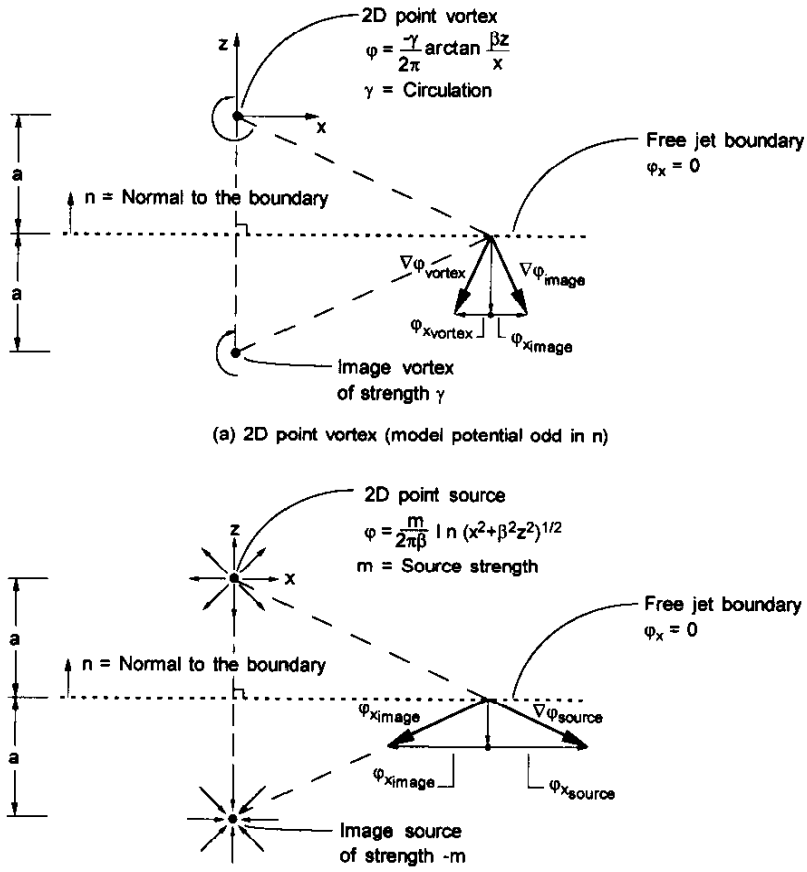

Figure 2.4 Method of Images for a Planar Free-Jet Boundary

The application of the method of images to wall interference involves the development of the set of images required to represent all the wall surfaces of a given test section and summing their effect to determine the interference at the model. Symmetry considerations guide the construction of an image system.

The interference factors for a small model at the centre of a rectangular test section with either all closed or all free-jet boundaries are summarised in Figure 2.5. Circular test section values, indicated for reference, fall very close to square tunnel values.

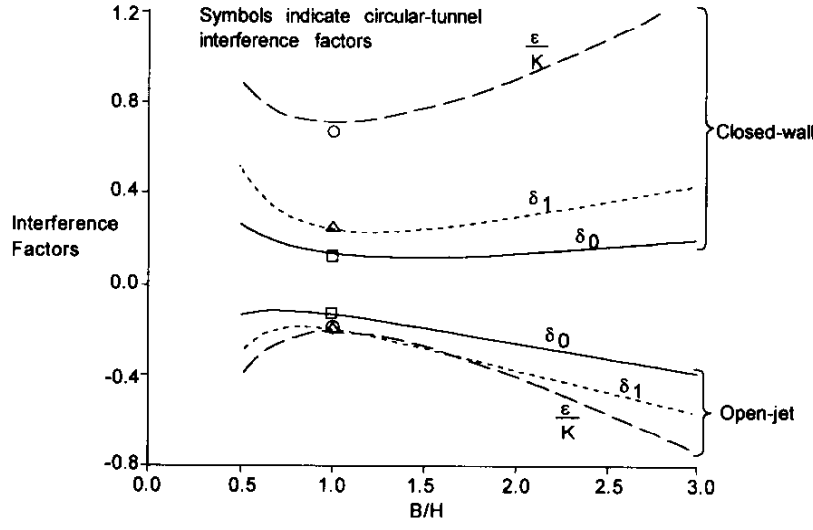

Figure 2.5 Classical Wall Interference Correction Factors for Small Models in Closed-Wall and Open-Jet Rectangular Tunnels

2.2 CLASSICAL CORRECTIONS FOR CLOSED TEST SECTIONS

Test sections with closed, planar, and aerodynamically parallel walls are perhaps the easiest to understand and analyse. The boundary condition for each wall lends itself to treatment by the method of images. The qualitative effects of these walls are predictable based on physical arguments alone, thus providing a common-sense validation of the analytic results. To be sure, the presence of more than one wall requires the use of multiple images. In fact, an infinite array of singularities is required even in the simplest case of two walls. Nonetheless, as has been shown in the literature, the infinite series representing the interference potential for small models in such tunnels converges quickly enough for ready calculation, especially given current computational capabilities.

In two dimensions, the closed-wall boundary condition can be satisfied on the upper and lower walls by using a single row of image singularities both above and below the test section. In constructing the image system each wall initially requires an image outside the test section of the model within the test section. However, the presence of the first-order singularity for the lower wall violates the parallel-flow boundary condition on the upper wall, thus requiring a second singularity above the ceiling, and similarly for the floor. For a model placed midway between the floor and ceiling this results in an infinite set of singularities, all at the same station as the model, equally spaced in z, aligned above and below the test section as indicated in Figure 2.6. A single infinite summation expresses the interference in the test section. This image system is readily generalised to the case of asymmetric model location.

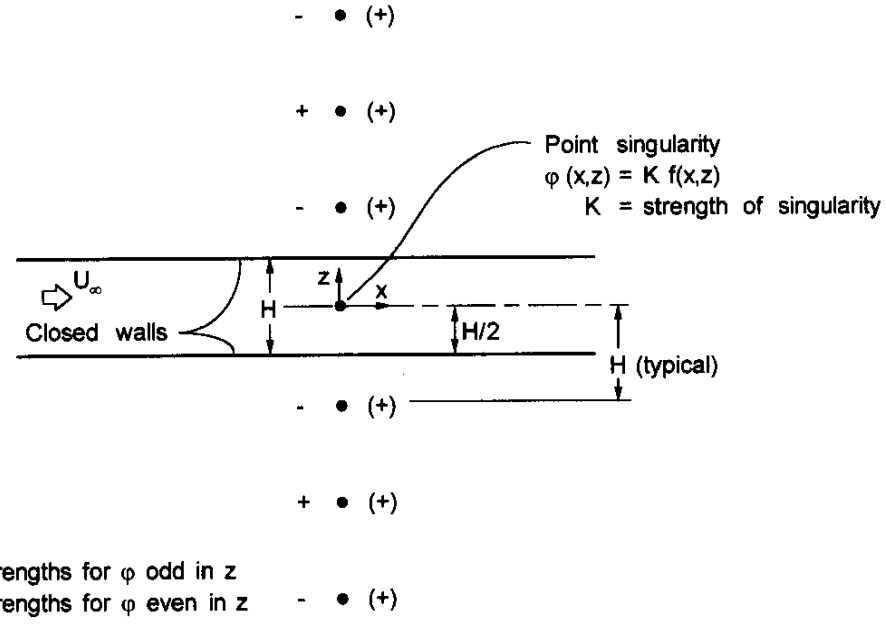

Figure 2.6 Image System for a Singularity at the Centre of a 2D Tunnel with Closed Walls

For the 3D testing situation in rectangular test sections, the image system becomes doubly infinite because of mutual interference of vertical and horizontal walls, which requires images along the diagonals, Figure 2.7. In general, this results in a double summation for the interference in the test section.

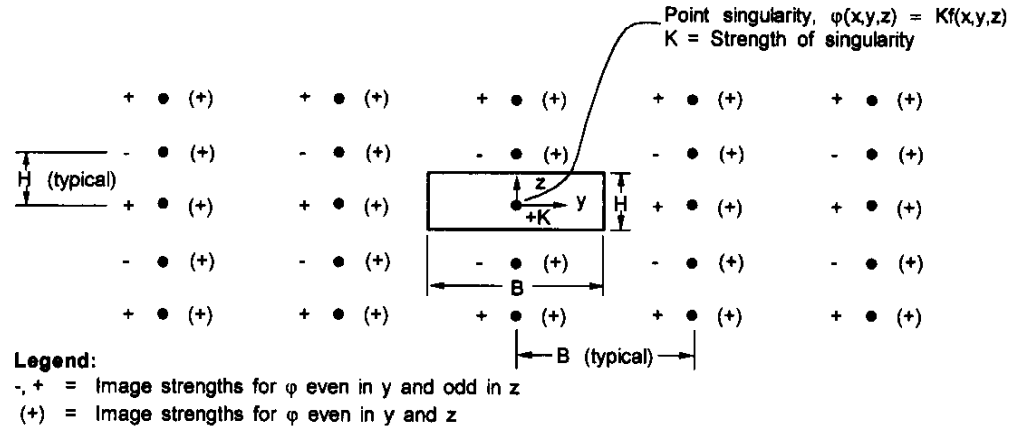

Figure 2.7 : Image System for a Model Singularity in the Centre of a 3D Rectangular Tunnel with Closed Walls

A particularly elegant image system in the crossflow plane far downstream of the bound vortex satisfies the boundary conditions for a closed-wall tunnel of circular cross section, Figure 2.8. This image system has been used to predict the upwash interference at the model, reasoning that the interference at the model location is half the interference value evaluated far downstream.

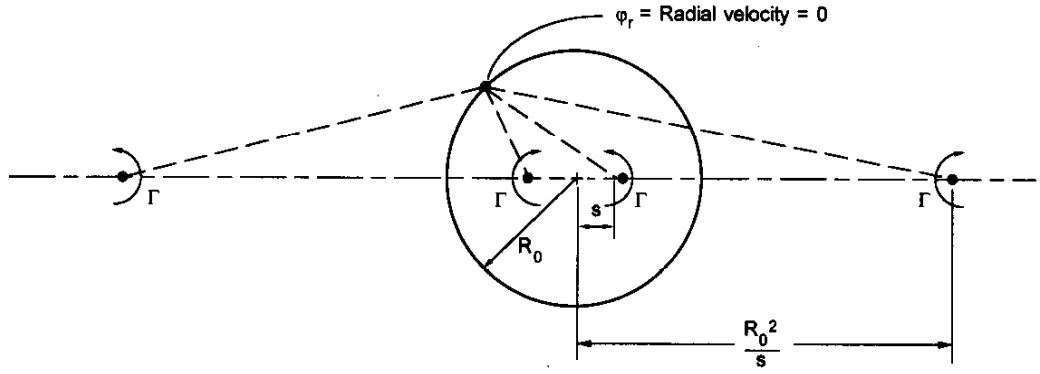

Figure 2.8 Image System for Trailing Vortices in a Tunnel of Circular Cross-Section

Early recognition of the limitations of single-singularity representations of model aerodynamics stimulated the development of multiple-singularity methods and applications, wherein elementary singularities are used as building blocks to represent the finite physical extent of the model. For a closed-wall rectangular tunnel, a complete image system can be specified for each singularity. By superposition, the collection of model singularities along with the corresponding sets of images will satisfy the wall boundary conditions.

All results presented in this section are for model singularities located on the centreline of the test section. Off-centreline model location involves appropriate generalisations of the image systems, resulting in both streamwise and upwash interference at the model location for any single type of singularity. 2D interference results are given throughout the test section, including both streamwise and upwash interference velocity components to highlight the qualitative features of interference variation that a large model at high incidence might experience. These features are mirrored in 3D testing, so that a large 3D model (length and span) may be viewed as immersed in a variable interference flow field. Tunnel users should be alert to the possibility that remote locations of a large model (e.g., outboard wing, body nose, and tail) may experience significantly different interference than predicted at the model

nominal reference location (often taken as the quarter-chord of the mean aerodynamic chord of the wing). 3D interference results presented here are limited to the main results: streamwise interference for the source singularities and upwash interference for the vortex singularities.

2.2.1 CLASSICAL CORRECTIONS FOR LIFT INTERFERENCE

Lift interference is defined to be that part of the wall interference due to circulation (i.e., corresponding to a force normal to the oncoming stream direction) generated by the model. For a small model centrally located in a test section, the model lift results in primarily an upwash interference in the vicinity of the model. Typically, this change in effective freestream direction directly modifies the model aerodynamic angle of attack and requires the resolution of force balance measurements relative to the corrected wind axis direction.

2.2.1.1 2D LIFT INTERFERENCE

In 2D flow, a point vortex singularity is used to represent the lifting effect of an airfoil. The potential for a point vortex located at $x=z=0$ is

$$\varphi_m = -\frac{\gamma}{2\pi}\arctan\left(\frac{\beta z}{x}\right) \tag{2.12}$$

where γ, the vortex strength, is 1/2 $U_\infty cC_L$ and c is the airfoil chord. Defining nondimensional spatial coordinates $\xi=x/\beta H$ and $\zeta=z/H$, the upwash interference anywhere in the tunnel for a model centrally located between closed upper and lower walls is given by

$$\delta(\xi,\zeta) = \frac{H}{U_\infty cC_L}\frac{\partial\varphi_w}{\partial z} = -\frac{1}{4\pi}\sum_{\substack{n=-\infty \\ n\neq 0}}^{n=\infty}(-1)^n\frac{\xi}{\xi^2+(\zeta-n)^2} \tag{2.13}$$

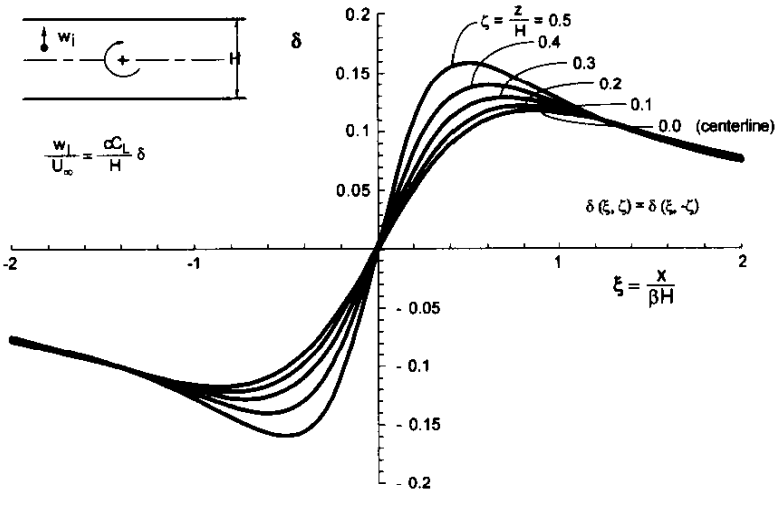

Figure 2.9 Upwash Interference of a 2D Vortex in a Closed-Wall Tunnel

The upwash interference throughout the test section is shown in Figure 2.9. It is zero at the model station as expected, since the velocity due to each image singularity is in the streamwise direction at this station. The upwash gradient, however, is not zero, so that a model will experience additional lift due to this induced camber relative to the interference-free case. The streamwise curvature interference parameter at the model location ($\xi=\zeta=0$) is

$$\delta_1(0,0)=\left.\frac{\partial\delta}{\partial\xi}\right|_{0,0}=-\frac{1}{4\pi}\sum_{\substack{n=-\infty\\ n\neq 0}}^{n=\infty}(-1)^n\frac{1}{n^2}=\frac{\pi}{24} \tag{2.14}$$

Since the upwash gradient is proportional to C_L, the uncorrected lift curve will be steeper.

For convenience, a streamwise interference parameter (due to lift) can be defined as

$$\varepsilon_\delta(\xi,\zeta)=\frac{H}{U_\infty cC_L}\frac{\partial\varphi_w}{\partial x}=\frac{1}{4\pi\beta}\sum_{\substack{n=-\infty\\ n\neq 0}}^{n=\infty}(-1)^n\frac{\zeta-n}{\xi^2+(\zeta-n)^2} \tag{2.15}$$

By symmetry, the streamwise interference is identically zero along the tunnel axis, being positive above the axis and negative below the axis at the model station (for positive lift), Figure 2.10. Far upstream and downstream of the model, both the streamwise and upwash interference velocities approach zero.

Although these results are strictly applicable only to a small model, the implications of finite model size are apparent from consideration of the spatial variations of interference velocities in Figures 2.9 and 2.10. A model centred between the walls at zero incidence may have a chord length that places leading and trailing edges beyond the region of "constant" interference. Further, rotating such a model through a range of incidence angles moves both leading and trailing edges away from the centreline and into regions of variable upwash and streamwise interference. The limits of linear streamwise upwash along the centreline are no more than about $x/\beta H \leq \pm 0.4$, Figure 2.10. Deviations of both upwash and streamwise interference from the centreline value are small for $z/H \leq \pm 0.2$.

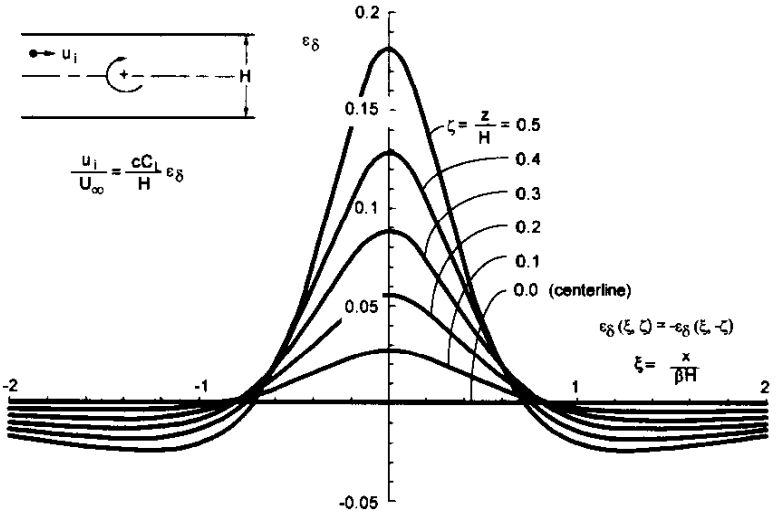

Figure 2.10 Streamwise Interference of a 2D Vortex in a Closed-Wall Tunnel

For a small model centrally located between two closed parallel walls, Allen and Vincenti [3] provide the following corrections due to flow curvature. These take account of the actual centre of lift of the model through inclusion of the pitching moment, C_M.

$$\Delta\alpha=\frac{\pi c^2}{96\beta H^2}\left(C_L+4C_M\right) \tag{2.16}$$

$$\Delta C_L=-\frac{\pi^2}{48}\left(\frac{c}{\beta H}\right)^2 C_L \tag{2.17}$$

$$\Delta C_M=\frac{\pi^2}{192}\left(\frac{c}{\beta H}\right)^2 C_L \tag{2.18}$$

These results were derived for an arbitrary chordwise loading (expressed in terms of a Fourier sine series plus a cotangent term to represent the flat plate loading), and are based on the idea of matching suction peaks in the tunnel and in free air. $\Delta\alpha$ is evaluated at the midchord; ΔC_L and ΔC_M represent the linearised loading changes due to the upwash variation over the chord. These corrections are consistent with the classical result of evaluating the angle of incidence correction at the ¾ chord for a set of corrections at constant lift (i.e., ΔC_L=0). Alternatively, for no change in pitching moment (ΔC_M=0), the angle of incidence correction should be evaluated at the trailing edge of the airfoil.

The case of off-centre model vortex location is summarised in Chapter II of AGARDograph 109 [13]; quoted results are based on Batchelor [8]. The upwash interference for a vortex located at $x=x_1$ ($\xi=\xi_1$) and $z=d-H/2$ (a distance d from the floor) in a 2D closed-wall tunnel is given as

$$\delta\left(\xi-\xi_1,\frac{d}{H}-\frac{1}{2}\right)=\frac{1}{4\pi}\left\{\sum_{n=-\infty}^{n=\infty}\frac{\xi-\xi_1}{\left(\xi-\xi_1\right)^2+4\left(n-d/H\right)^2}-2\sum_{n=1}^{n=\infty}\frac{\xi-\xi_1}{\left(\xi-\xi_1\right)^2+4n^2}\right\} \tag{2.19}$$

At a small streamwise distance, $\xi-\xi_1$, from the vortex, ignoring terms of order $(\xi-\xi_1)^3$, this can be approximated as

$$\delta\left(\xi-\xi_1,\frac{d}{H}-\frac{1}{2}\right)=\frac{\pi}{16}\left(\xi-\xi_1\right)\left(\frac{2}{3}+\cot^2\frac{\pi d}{H}\right) \tag{2.20}$$

If the vortex represents the lift of an airfoil acting at the centre of pressure, then for pitching moment defined about the quarter-chord, the centre of pressure is located at a distance downstream of the leading edge,

$$\frac{x_1}{c}=\frac{1}{4}-\frac{C_M}{C_L} \tag{2.21}$$

and the upwash interference can be expressed as

$$\delta\left(\frac{x}{c},\frac{d}{H}-\frac{1}{2}\right)=\frac{\pi}{16\beta}\frac{c}{H}\left\{\left(\frac{x}{c}-\frac{1}{4}\right)-\frac{C_M}{C_L}\right\}\left(\frac{2}{3}+\cot^2\frac{\pi d}{H}\right) \tag{2.22}$$

Batchelor also derives the streamwise interference velocity at the vortex as

$$\varepsilon\left(\xi=\xi_1,\zeta=\frac{d}{H}-\frac{1}{2}\right)=\frac{u_i}{U_\infty}=-\frac{1}{8\beta}\frac{c}{H}C_L\cot\frac{\pi d}{H} \tag{2.23}$$

Thus, the streamwise interference is identically zero only for a centrally located vortex. Otherwise, it is either positive or negative according to whether the vortex is above or below the test section centreline (as can be inferred from consideration of the incremental effects of the nearest image vortices). These results are analogous to the interference of a centrally located vortex evaluated off-centreline, Figure 2.9.

The above summarises corrections due to lift in a 2D closed-wall tunnel to order $(c/H)^2$. AGARDograph 109 [13] includes a discussion of higher order correction theory (to order $(c/H)^4$), concluding that the lower order results are inaccurate for $c>0.4\beta H$. For a model centrally located between two closed walls, the following corrections are presented based on Havelock [17], ignoring terms of order $(c/\beta H)^6$,

$$\Delta\alpha=\frac{\pi c^2}{96\beta H^2}\left(C_L+4C_M\right)-\frac{7\pi^3c^4C_L}{30720\beta^3H^4} \tag{2.24}$$

$$\Delta C_L = C_L\left\{-\frac{\pi^2}{48}\left(\frac{c}{\beta H}\right)^2+\frac{7\pi^4}{3072}\left(\frac{c}{\beta H}\right)^4\right\} \tag{2.25}$$

$$\Delta C_M = C_L\left\{\frac{\pi^2}{192}\left(\frac{c}{\beta H}\right)^2-\frac{7\pi^4}{15360}\left(\frac{c}{\beta H}\right)^4\right\} \tag{2.26}$$

The general problem of a thick airfoil has been solved by Goldstein [16] as a power series in (*c/H*) by transforming the airfoil to a circle, and is summarised in AGARDograph 109 [13]. This solution is consistent with the above results when second-order terms in thickness, camber, and incidence are ignored.

2.2.1.2 3D Lift Interference for Small Wings

The lift of a small model can be simulated using an elementary horseshoe vortex of span *2s* (equivalent to a line doublet), whose potential is given by

$$\varphi_m = \frac{\Gamma s}{2\pi}\left[1+\frac{x}{\left(x^2+\beta^2 r^2\right)^{\frac{1}{2}}}\right]\left[\frac{z}{y^2+z^2}\right] \tag{2.27}$$

where the vortex strength (Γs) is 1/4 U_∞ S C_L, S is the reference area of the wing, and r is the radial cylindrical co-ordinate, $\sqrt{y^2+z^2}$. The upwash velocity field is then

$$\frac{\partial\varphi_m}{\partial z} = \frac{\Gamma s}{2\pi}\left\{\left[1+\frac{x}{\left(x^2+\beta^2y^2+\beta^2z^2\right)^{\frac{1}{2}}}\right]\left[\frac{y^2-z^2}{\left(y^2+z^2\right)^2}\right]-\frac{\beta^2xz^2}{\left(x^2+\beta^2y^2+\beta^2z^2\right)^{\frac{3}{2}}\left(y^2+z^2\right)}\right\} \tag{2.28}$$

In the plane of the bound vortex normal to the oncoming stream (that is, for *x=0*) the upwash takes on the simple form

$$w(0,y,z) = \frac{\Gamma s}{2\pi}\left\{\frac{y^2-z^2}{\left(y^2+z^2\right)^2}\right\} \tag{2.29}$$

For rectangular tunnels, the image system is a 2D array as discussed in Section 2.1.3. Defining the aspect ratio of the tunnel as *A=B/H* and evaluating the upwash interference at the model location, *x=y=z=0*, the classical result is recovered:

$$\delta_o = \delta(0,0,0) = \frac{A}{8\pi}\sum_{\substack{n=-\infty \\ \text{excluding} \\ n=m=0}}^{n=\infty}\sum_{m=-\infty}^{m=\infty}(-1)^n\frac{m^2A^2-n^2}{\left[m^2A^2+n^2\right]^2} \tag{2.30}$$

Differentiating (with respect to $x/\beta H$) the expression for upwash interference due to the infinitesimal horseshoe vortex, the analogous expression for upwash gradient at the model location is derived:

$$\delta_1(0,0,0) = \left.\frac{\partial\delta}{\partial(x/\beta H)}\right|_{0,0,0} = \frac{A}{8\pi}\sum_{\substack{n=-\infty \\ \text{excluding} \\ n=m=0}}^{n=\infty}\sum_{m=-\infty}^{m=\infty}(-1)^n\frac{m^2A^2-2n^2}{\left[m^2A^2+n^2\right]^{\frac{5}{2}}} \qquad (2.31)$$

As developed by Theodorsen [34], similar expressions apply to the upwash interference in rectangular tunnels having all open walls, open sides and closed floor and roof, and closed sides and open floor and roof. Because the image systems for these cases require only appropriate sign changes (see Glauert, Figs. 7 and 8), the factor $(-1)^n$ should be replaced by $(-1)^m$, $(-1)^{m+n}$, and (1), respectively; see Section 4.1.2.4 (Fig. 4.4).

Along the centreline of rectangular tunnels, the upwash interference asymptotically approaches zero in the upstream direction and a constant positive value in the downstream direction, Figure 2.11. The interference upwash far downstream of the model is due to the image trailing vorticity, which (at this

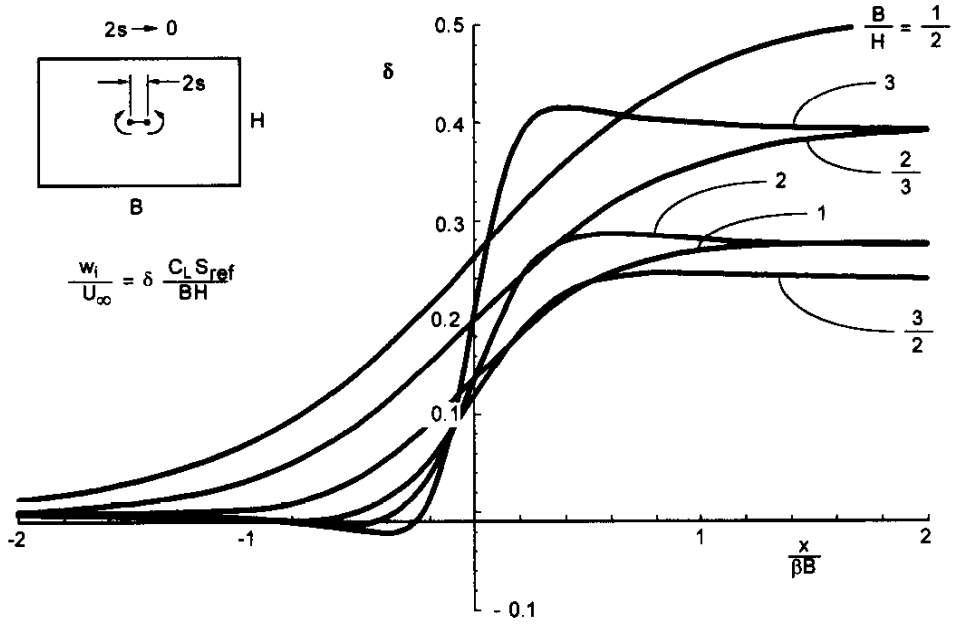

Figure 2.11 Centreline Distribution of Upwash Interference of an Elementary Horseshoe Vortex in Closed-Wall Rectangular Tunnels

location) extends effectively to infinity in both directions. At the model location, the image bound vortex segments do not induce any upwash (as in the 2D case). Because the image trailing vortex segments extend only downstream from the model location, by symmetry the upwash interference at the model is therefore exactly half the value of the downstream asymptotic interference. The spanwise variation of upwash interference, Figure 2.12, is significantly greater for tunnels having $A > 3/2$. The magnitude of interference at the model location increases for $A < 1$. From the standpoint of both small magnitude and minimum spanwise variation, near-optimum upwash interference is obtained for $1 \leq A \leq 3/2$. These small-span results indicate the nature of the interference-gradient problems that will occur for finite-span wings.

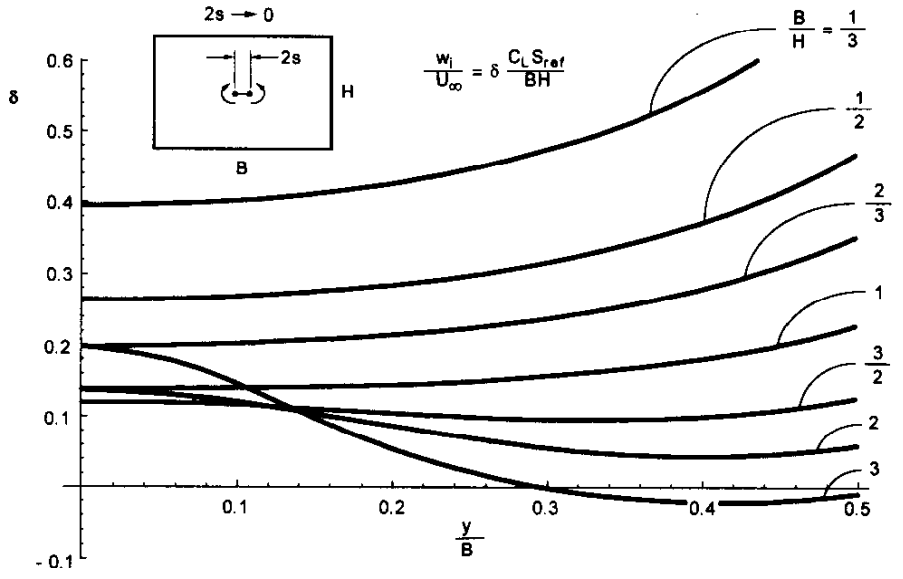

Figure 2.12 Spanwise Distribution of Upwash Interference of an Elementary Horseshoe Vortex in Closed-Wall Rectangular Tunnels

2.2.1.3 3D Lift Interference for Wings of Finite Span

The effect of finite span of the horseshoe vortex on upwash interference provides the next logical approximation to the interference of a wing. A straight unswept wing having a small chord, finite span and uniform span loading can be represented by a finite-span horseshoe vortex, whose velocity potential is (see Ashley and Landahl, [5])

$$\varphi_m = \frac{1}{4\pi}\int_{-s}^{s} \frac{\Gamma z}{(y-y_1)^2+z^2}\left[1+\frac{x}{R(y-y_1)}\right]dy_1$$
$$= \frac{\Gamma s}{2\pi}\left\{\arctan\left(\frac{z}{y-s}\right) - \arctan\left(\frac{z}{y+s}\right) - \arctan\left(\frac{x(y-s)}{zR(y-s)}\right) + \arctan\left(\frac{x(y+s)}{zR(y+s)}\right)\right\} \quad (2.32)$$

where $R(y) = \sqrt{x^2+\beta^2y^2+\beta^2z^2}$.

Differentiating this expression, the upwash velocity is

$$\frac{\partial\varphi}{\partial z} = \frac{\Gamma s}{2\pi U_\infty}\left\{\begin{array}{l} \dfrac{y-s}{(y-s)^2+z^2} - \dfrac{y+s}{(y+s)^2+z^2} \\ + \dfrac{x(y-s)\left(x^2+\beta^2(y-s)^2+2\beta^2z^2\right)}{z^2\left(R(y-s)\right)^{\frac{3}{2}}T(y-s)} - \dfrac{x(y+s)\left(x^2+\beta^2(y+s)^2+2\beta^2z^2\right)}{z^2\left(R(y+s)\right)^{\frac{3}{2}}T(y+s)} \end{array}\right\} \quad (2.33)$$

where T is defined as

$$T(y) = 1 + \frac{x^2 y^2}{z^2\left(x^2 + \beta^2 y^2 + \beta^2 z^2\right)} \tag{2.34}$$

For a finite-span 3D wing it is convenient to define nondimensional co-ordinates using the tunnel breadth: $\xi = x/\beta B$, $\eta = y/B$, and $\zeta = z/B$, and a nondimensional semispan, $\sigma = s/B$. In the plane of the bound vortex, $\xi = \zeta = 0$, the upwash interference of a finite-span horseshoe vortex in a rectangular tunnel ($A = B/H$ as before) is given by the double summation of the image system,

$$\delta(0,\eta,0) = \frac{A}{16\pi\sigma} \sum_{\substack{n=-\infty \\ \text{excluding} \\ n=m=0}}^{n=\infty} \sum_{m=-\infty}^{m=\infty} (-1)^n \left\{ \frac{\eta - \sigma - m}{A^2(\eta - \sigma - m)^2 + n^2} - \frac{\eta + \sigma - m}{A^2(\eta + \sigma - m)^2 + n^2} \right\} \tag{2.35}$$

For wings of finite span, upwash interference along the centreline of rectangular tunnels, Figure 2.13, qualitatively mirrors the interference of models of small span. Upwash interference variation along the span of the bound vortex in a square closed-wall tunnel is shown in Figure 2.14. As span increases, the average upwash interference at the centre of the model ($\xi = \eta = \zeta = 0$) increases. More important, however, is the increased spanwise variation of interference due to span. This is manifested as increased upwash on the outboard wing with increasing span ratio (due to the increasing proximity of the first set of image trailing vortex segments). The effect of span can be ignored for span ratios less than about 0.5.

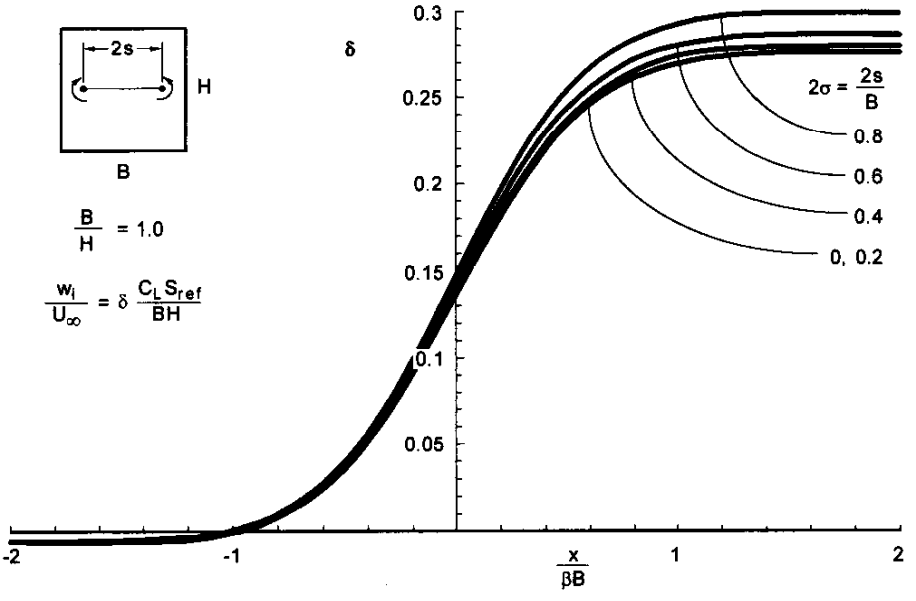

Figure 2.13 Streamwise Interference of a 2D Source Doublet in a Closed-Wall Tunnel

An extensive series of lift interference charts for rectangular and elliptic closed-wall tunnels, including the effects of finite span, uniform versus elliptic span loading, and off-centre wing location, are presented in Pope and Harper [31]. The rapid rollup of trailing vorticity of a finite-span wing into two concentrated trailing vortices duplicates the trailing vortex pattern for uniform loading. The distance between these concentrated trailing vortices, the so-called vortex span, is given as a function of wing aspect and taper ratios. The interference at the wing can be estimated using an effective vortex span smaller than the physical span, but larger than the rollup vortex span. For wings of small span to tunnel width ratio, a

simple average of the physical and rollup vortex span results in negligible error. Large span wings or very exacting correction requirements may demand the consideration of actual spanload.

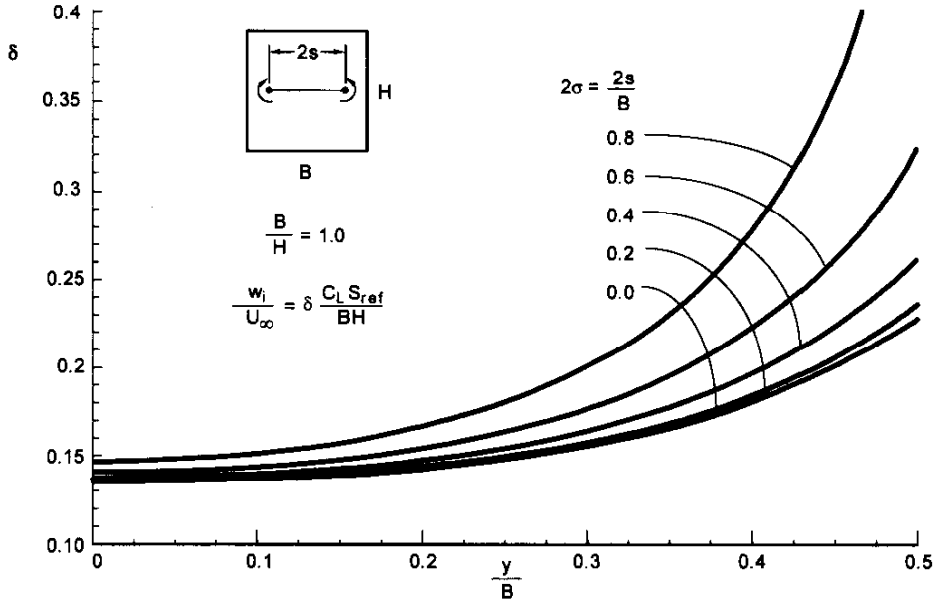

Figure 2.14 Upwash Interference of a 2D Source Doublet in a Closed-Wall Tunnel

2.2.1.4 APPLICATION OF UPWASH CORRECTIONS

Additional upwash at the model location due to the walls requires corrections to angle of attack and drag (due to the change in effective stream direction at the model location, and to pitching moment and lift (or to pitching moment and angle of attack) due to the streamwise gradient of the interference upwash). For a small model and small upwash angle, the corrections to lift and drag due to the former (i.e., rotation of wind axes) are

$$C_{Lcorr} = C_{Lunc}\cos\Delta\alpha - C_{Dunc}\sin\Delta\alpha \cong C_{Lunc} \tag{2.36}$$

$$C_{Dcorr} = C_{Dunc}\cos\Delta\alpha + C_{Lunc}\sin\Delta\alpha \cong C_{Dunc} + C_{Lunc}\Delta\alpha \tag{2.37}$$

$$\Delta\alpha = \delta_o \frac{S}{C} C_{Lunc} \tag{2.38}$$

where $\Delta\alpha$ is evaluated at the model centre of lift (nominally the wing quarter-chord location).

Though the above relationships define a corrected onset stream direction, the model angle of attack must additionally be adjusted for interference stream curvature. Because the wing is immersed in an interference flow field characterised by increasing upwash with x, it appears to have an increased effective camber (in a closed-wall tunnel) compared to an unbounded flow. Corrections for this flow curvature may be applied to pitching moment and to either (or both) lift coefficient or angle of attack. It is perhaps most convenient to consider this flow-induced camber as an additional model incidence (though not to be included in the stream angle change for redefining wind axes) with no adjustment to lift and an additional pitching moment due to this camber that would not occur in an unbounded stream. For a linear longitudinal variation of interference upwash, and relying on linearised airfoil theory results for a

circular-arc airfoil (see Glauert, [15]; or Pope, [31]), the effective increase in incidence is accounted for if the upwash is evaluated at the 3/4-chord location (rather than the quarter-chord, which coincides with the centre of lift in linear theory). In terms of $\Delta\alpha$, δ_o, and δ_1 evaluated at the location of the bound vortex,

$$\alpha_{corr} = \alpha_{unc} + \Delta\alpha + \Delta\alpha_{sc} = \alpha_{unc} + \left(\delta_o + \frac{\bar{c}}{2\beta H}\delta_1\right)\frac{SC_{Lunc}}{C} \tag{2.39}$$

The pitching moment correction is

$$\Delta C_M = \delta_1 \frac{\bar{c}}{16\beta H}\frac{SC_{Lunc}}{C}\frac{\partial C_L}{\partial \alpha} \tag{2.40}$$

For the 2D case, S and C are replaced by c and H respectively.

For wings of finite span and arbitrary spanwise loading, the average interference upwash (δ_o, in nondimensional terms) can be taken to be the loading-averaged upwash as given in AGARDograph 109,

$$\delta_o = \frac{1}{L}\int_{-s}^{s}\left(\frac{w_i}{U_\infty}\frac{C}{SC_L}\right)\frac{dL}{dy}dy \tag{2.41}$$

2.2.2 Classical Corrections for Blockage Interference

Blockage interference is that part of the wall interference due to the displacement of streamlines around a body that carries no lift or side force. Solid blockage represents that part of the blockage due to the volume of the model in the tunnel. This is usually taken to be a closed body, though if the effect of a support sting is sought, under certain circumstances modelling of its volume might take the form of a semi-infinite body which can be represented by a source. A source flow is similarly used to represent the displacement effect of a viscous wake from the model.

2.2.2.1 2D Solid Blockage For Small Models

As discussed by Glauert [15], the flow field around any nonlifting body may be represented by a power series in the inverse of the complex spatial co-ordinate. At a large distance from the body, the leading term (of the form of a source doublet) dominates. In 2D flow, the potential of a source doublet is

$$\varphi_m = \frac{\mu}{2\pi}\left(\frac{x}{x^2 + \beta^2 z^2}\right) \tag{2.42}$$

In a uniform unconstrained stream, the potential of a source doublet aligned with the oncoming stream represents the flow around a cylinder whose radius (a) is related to the doublet strength,

$$\mu = \left(\frac{2\pi a^2 U_\infty}{\beta}\right) \tag{2.43}$$

The far field of any nonlifting body is approximated by this first-order term if μ is taken as AU_∞/β, where A is the effective cross-sectional area of the model. It is the sum of the model volume (per unit span) and its virtual volume (per unit span) for accelerated flow in the streamwise direction. Using nondimensional

co-ordinates $\xi=x/\beta H$, $\zeta=z/H$, and summing the effect of all the image doublets, the streamwise interference anywhere in the tunnel for a model centrally located between closed upper and lower walls is given by

$$\varepsilon = \frac{u_i}{U_\infty} = -\frac{1}{2\pi\beta^3}\frac{A}{c^2}\left(\frac{c}{H}\right)^2 \sum_{\substack{-\infty \\ n\neq 0}}^{\infty} \frac{\xi^2 - (\zeta - n)^2}{\left[\xi^2 + (\zeta - n)^2\right]^2} \tag{2.44}$$

It should be noted that at any value of ζ, the interference is a maximum at the model location, Figure 2.15, which increases the effective freestream velocity felt by the model. However, due to the streamwise symmetry of the interference, there is no pressure buoyancy force on the model.

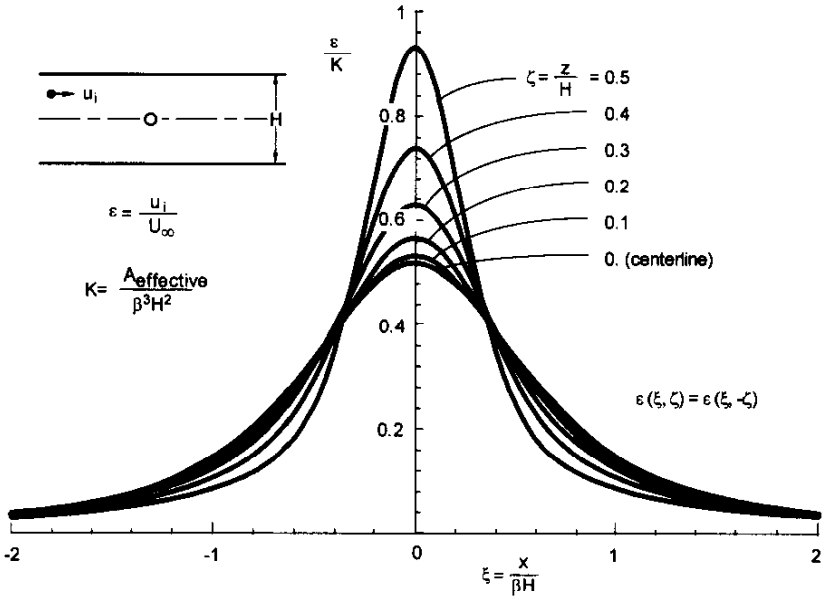

Figure 2.15 Streamwise Interference of a 2D Source Doublet in a Closed-Wall Tunnel

At the model location, $\xi=\zeta=0$, the interference is given by

$$\varepsilon(0,0) \equiv \varepsilon_0 = \frac{1}{2\pi\beta^3}\frac{A}{c^2}\left(\frac{c}{H}\right)^2 \sum_{\substack{n=-\infty \\ n\neq 0}}^{n=\infty} \frac{1}{n^2} = \frac{\pi}{6}\frac{A}{\beta^3 H^2} \tag{2.45}$$

As for the point vortex, interference at the model station is a minimum on centreline, with interference velocities for $z/H \leq 0.2x/\beta H$ very close to centreline values.

In a manner analogous to the point vortex, an upwash interference parameter for a nonlifting body can be defined :

$$\delta_\varepsilon(\xi,\zeta) = \frac{w_i}{U_\infty} = \frac{1}{U_\infty}\frac{\partial \varphi_w}{\partial z} = \frac{1}{2\pi\beta^2}\frac{A}{H^2} \sum_{\substack{n=-\infty \\ n\neq 0}}^{n=\infty} \frac{2\xi(\zeta - n)}{\left(\xi^2 + (\zeta - n)^2\right)^2} \tag{2.46}$$

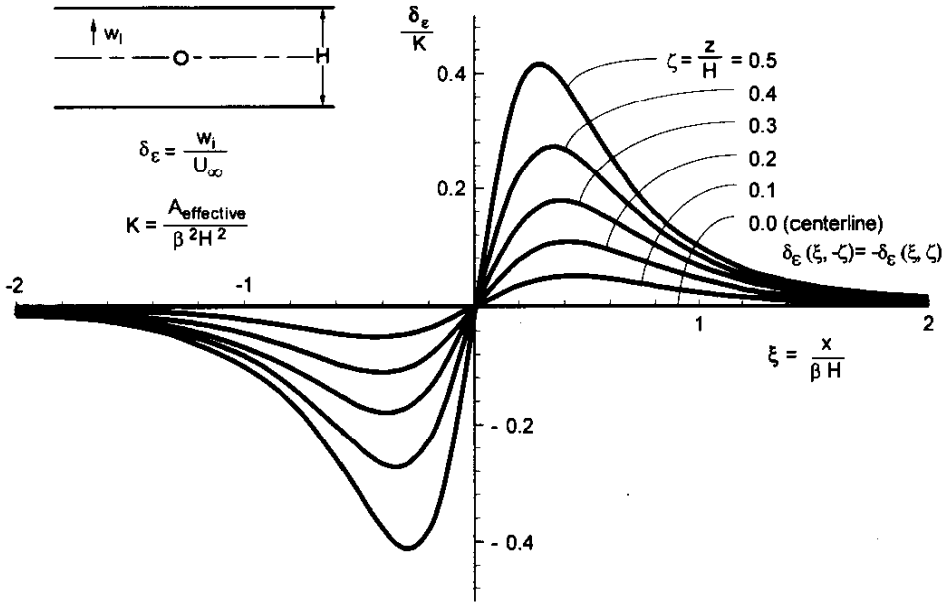

Figure 2.16 Upwash Interference of a 2D Source Doublet in a Closed-Wall Tunnel

By symmetry, the interference upwash due to solid blockage is zero along the axis of the tunnel, Figure 2.16. Off-centreline the interference upwash has a character similar to the upwash interference of a 2D vortex (Fig. 2.9).

Following Glauert [15], the effective cross-sectional area of any 2D body may be written in terms of an equivalent cylinder by defining a body shape factor, λ,

$$\mu = \frac{\pi}{2}\lambda t^2 U_\infty \tag{2.47}$$

so that the body is represented as an equivalent cylinder of diameter $t\sqrt{\lambda}$. Values of λ as a function of fineness ratio (c/t) are given by Glauert for several shapes: Rankine oval, ellipse, Joukowski section, and a modified Joukowski section. Pope [31] provides shape factors for several NACA airfoil series as well. The shape factor for an ellipse is described by a simple analytic expression,

$$\lambda = \frac{1}{2}\left(1 + \frac{c}{t}\right) \tag{2.48}$$

An alternate body shape factor may be defined by taking the effective cross-sectional area (A) to be $K A_0$, where K is a nondimensional factor depending on body shape and A_0 is the actual cross-sectional area. For an ellipse,

$$K = 1 + \frac{t}{c} \tag{2.49}$$

As fineness ratio increases, K approaches *1* and effective area is essentially the actual cross-sectional area. The more blunt the body, the larger is the effective area. A circle, for example, has an effective area twice its actual cross-sectional area.

In general, the effective cross-sectional area can be calculated for a symmetrical body from the surface velocity distribution, *V(s)*,

$$\lambda = \frac{4}{\pi} \int_{\text{leading edge}}^{\text{trailing edge}} \frac{V(s)}{U_\infty} \frac{z(s)}{t^2} ds \tag{2.50}$$

Glauert also provides a useful first approximation to λ, for cases when more reliable values are not available,

$$\lambda = \frac{2A_0}{\pi t^2} \tag{2.51}$$

The effect of thickness and angle of attack on blockage interference may be estimated using a general relationship suggested in AGARDograph 109 based on theoretical and empirical investigations,

$$\varepsilon_0 = \frac{\pi}{6}\left[1 + 1.2\beta\left(\frac{t}{c}\right)\right]\left[1 + 1.1\left(\frac{c}{t}\right)\alpha^2\right]\frac{A_0}{\beta^3 H^2} \tag{2.52}$$

2.2.2.2 2D RANKINE OVALS

A source and a sink located a finite distance apart (*2s*) on a line parallel to the oncoming stream have a streamline forming a closed body known in 2D flow as a Rankine oval (in 3D the analogous closed stream surface is referred to as a Rankine body). This simple superposition of singularities illustrates the effect of body length on solid blockage. The potential is given by

$$\varphi_m = \frac{m}{2\pi\beta}\left[\ln\left((x+s)^2 + \beta^2 z^2\right)^{\frac{1}{2}} - \ln\left((x-s)^2 + \beta^2 z^2\right)^{\frac{1}{2}}\right] \tag{2.53}$$

In terms of nondimensional co-ordinates $\xi = x/\beta H$, $\zeta = z/H$, and defining $\sigma = s/\beta H$, the streamwise interference is the sum of all images in the usual way,

$$\varepsilon = \frac{m}{2\pi\beta^2}\frac{c}{H}\sum_{\substack{n=-\infty \\ n\neq 0}}^{\infty}\left[\frac{\xi+\sigma}{(\xi+\sigma)^2 + (\zeta-n)^2} - \frac{\xi-\sigma}{(\xi-\sigma)^2 + (\zeta-n)^2}\right] \tag{2.54}$$

The streamwise interference of Rankine ovals having a maximum thickness *t/H=0.1* is shown in Figure 2.17. At small length ratios the interference is indistinguishable from that of a source doublet. Two features characterise the interference as the length of the model increases. First, the interference at the model leading and trailing edges decreases relative to the interference at the model centre. Second, the interference at the centre decreases as the flow in the tunnel approaches the 1D limit for very long models.

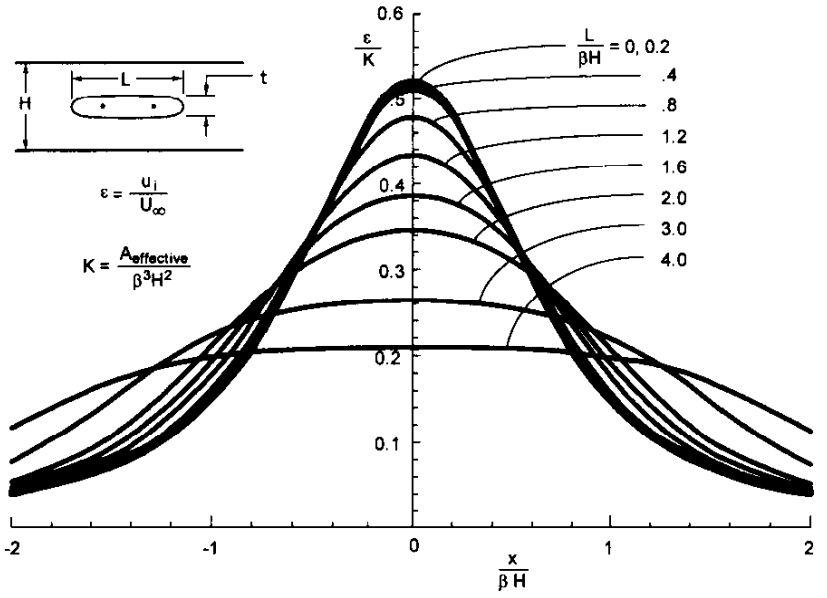

Figure 2.17 Streamwise Interference of Rankine Ovals (t/H = 0.1) in a Closed-Wall Tunnel

2.2.2.3 2D WAKE BLOCKAGE

In 2D flow the potential of a point source located at the origin is

$$\varphi_m = \frac{m}{2\pi\beta}\ln\left(x^2+\beta^2 z^2\right)^{\frac{1}{2}} \tag{2.55}$$

where m, the source strength, is 1/2 U_∞ c C_D. In terms of nondimensional co-ordinates $\xi=x/\beta H$ and $\zeta=z/H$, the streamwise interference anywhere in the tunnel for a model centrally located between closed upper and lower walls is given by

$$\varepsilon = \frac{C_D}{4\pi\beta^2}\frac{c}{H}\sum_{\substack{-\infty\\ n\neq 0}}^{\infty}\frac{\xi}{\xi^2+\left(\zeta-n\right)^2} \tag{2.56}$$

The streamwise interference attains its maximum value far downstream of the model location, Figure 2.18. Its magnitude is consistent with 1D streamtube considerations: downstream of the model, the tunnel cross-sectional area is decreased by the equivalent displacement area of the viscous wake plume, so that the flow external to the wake must increase proportionately. In total, the image sources add additional mass to the oncoming stream, so that the uniform velocities far upstream and downstream cannot be equal. An interesting result for this singularity set is the non-zero interference far upstream of the model. Formally, this physical paradox can be alleviated by providing each source with a corresponding sink far downstream of the model, thus closing off each "wake body". This array of sinks produces an equal and opposite interference flow far upstream that restores the undisturbed onset stream velocity.

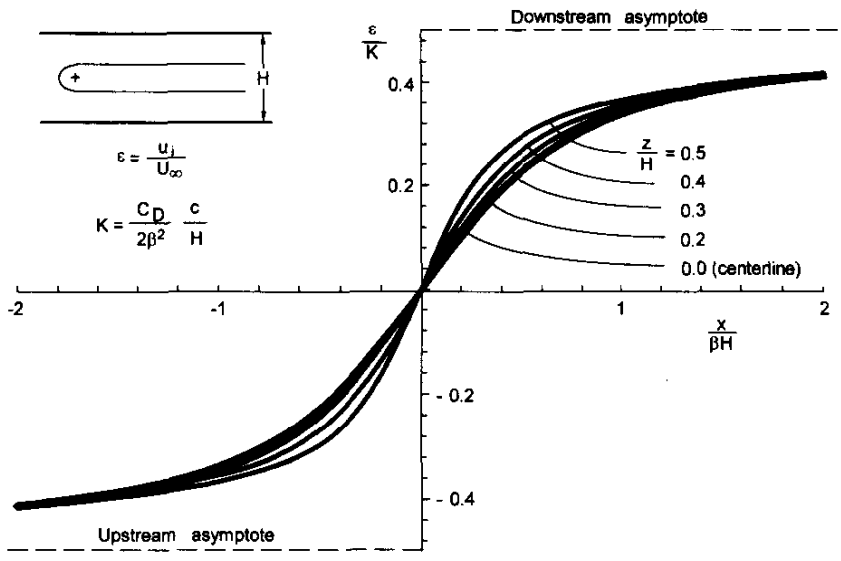

Figure 2.18 Streamwise Interference of a 2D Source in a Closed-Wall Tunnel

A practical approach to wake blockage corrections takes the upstream interference to be zero. Because the setting of tunnel speed commonly relies on a wall static pressure measurement upstream of the test section, the influence of the model at this location is automatically included in the definition of uncorrected tunnel speed. Therefore, the wake blockage interference at the model location should be taken as the difference between the interference at the static pressure reference location and the interference at the model location in Figure 2.18. If the upstream asymptote is used as a reference, the interference at the model is

$$\varepsilon_0 = \frac{C_D}{4\beta^2}\frac{c}{H} \tag{2.57}$$

The streamwise gradient of wake blockage interference is a maximum at the model location and results in a buoyancy force on the model. Differentiating the series expression for ε due to the source representing the displacement of the wake, the same series appears as for solid blockage of a source doublet, so that

$$\frac{\partial \varepsilon_{wake}}{\partial \xi} = \frac{C_D}{2}\frac{\beta H c}{A}\varepsilon_{solid} \tag{2.58}$$

At the model location, $\xi=\zeta=0$,

$$\frac{\partial \varepsilon_{wake}}{\partial \xi} = \frac{\pi}{12}\frac{C_D}{\beta^2}\frac{c}{H} \tag{2.59}$$

By symmetry, the interference upwash is zero along the axis of the tunnel and, in the vicinity of the model, the interference upwash is directed from the walls toward the tunnel axis.

2.2.2.4 3D SOLID BLOCKAGE FOR SMALL MODELS

In 3D flow, the potential of a source doublet is

$$\varphi_m = \frac{\mu}{4\pi} \frac{x}{\left(x^2 + \beta^2 r^2\right)^{\frac{3}{2}}} \tag{2.60}$$

where $r^2 = y^2 + z^2$ and the doublet strength, m, is $U_\infty V$, where V is the effective volume of the model. Analogous to the 2D source doublet, superposition of a 3D source doublet and a uniform oncoming stream represents the flow around a sphere whose radius (a) is related to the doublet strength by

$$\mu = 2\pi a^3 U_\infty \tag{2.61}$$

The streamwise velocity due to this singularity is

$$\frac{\partial \varphi}{\partial x} = -\frac{\mu}{4\pi} \left\{ \frac{2x^2 - \beta^2 r^2}{\left(x^2 + \beta^2 r^2\right)^{\frac{5}{2}}} \right\} \tag{2.62}$$

For a rectangular tunnel, an array of image doublets placed as for the lifting case (but, unlike the lifting case, all having the same sign) satisfies the closed-wall boundary condition at the walls. Using $L_{ref} = \sqrt{BH}$ as the reference length for nondimensional co-ordinates ($\xi = x/\beta L_{ref}$, $\eta = y/L_{ref}$, $\zeta = z/L_{ref}$), the streamwise interference anywhere in the tunnel for a model located in the centre of a rectangular test section is given by

$$\varepsilon = \frac{u_i}{U_\infty} = -\frac{A^{\frac{3}{2}}}{4\pi\beta^3} \frac{V}{(BH)^{3/2}} \sum_{\substack{n=-\infty \\ \text{excluding} \\ n=m=0}}^{n=\infty} \sum_{n=-\infty}^{m=\infty} \left\{ \frac{2\xi^2 - \left(\eta\sqrt{A} - mA\right)^2 - \left(\zeta\sqrt{A} - n^2\right)^2}{\left[\xi^2 + \left(\eta\sqrt{A} - mA\right)^2 + \left(\zeta\sqrt{A} - n\right)^2\right]^{\frac{5}{2}}} \right\} \tag{2.63}$$

As for the 2D case (Fig. 2.15) the streamwise interference is a maximum at the model location, Figure 2.19, which increases the effective free stream, but with no consequent pressure buoyancy effect on the model. By symmetry, the interference upwash is zero along the axis of the tunnel.

Evaluating the interference at the model location, $\xi = \eta = \zeta = 0$, the classical result is recovered,

$$\varepsilon_0 \equiv \varepsilon(0,0,0) = \frac{A^{\frac{3}{2}}}{4\pi} \frac{V}{\beta^3 (BH)^{3/2}} \sum_{\substack{n=-\infty \\ \text{excluding} \\ n=m=0}}^{n=\infty} \sum_{m=-\infty}^{m=\infty} \frac{1}{\left[m^2 A^2 + n^2\right]^{\frac{3}{2}}} \tag{2.64}$$

For an arbitrary axisymmetric body, a body shape factor, λ, is defined (per Lock [22]; also Glauert [15]) so that the blockage velocity is

$$\varepsilon_0 = \tau\lambda \left(\frac{A_{\text{maximum}}}{C} \right)^{3/2} \tag{2.65}$$

where C = tunnel area (= BH for a rectangular section), τ depends on the shape of the tunnel and λ on the shape of the body. Using this definition of λ, the far field is approximated by the flow around an equivalent sphere of diameter $t\lambda^{1/3}$, where t is the maximum body thickness.

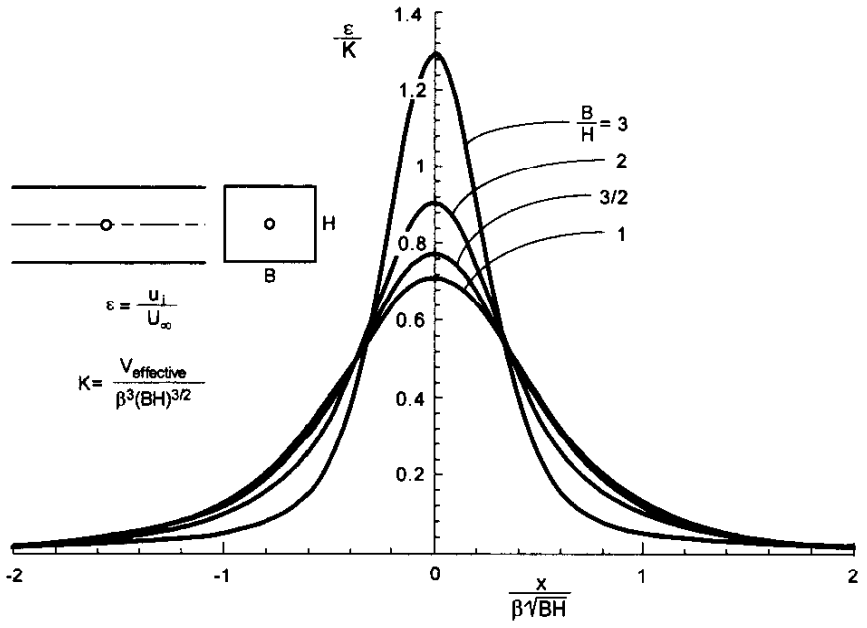

Figure 2.19 Centreline Distribution of Streamwise Interference of a 3D Source Doublet in Closed-Wall Rectangular Wind Tunnels

The effective volume can be calculated from the surface velocity distribution, *V(s)*, using

$$\lambda = 4 \int_{\text{leading edge}}^{\text{trailing edge}} \frac{V(s)}{U_\infty} \frac{[z(s)]^2}{t^3} ds \tag{2.66}$$

Glauert provides an approximation for the 3D case corresponding to Equation 2.51 in two dimensions,

$$\lambda = \frac{4V_0}{\pi t^3} \tag{2.67}$$

where V_0 is the body volume.

2.2.2.5 3D RANKINE BODIES

The effect of body length is illustrated by results for the Rankine body, which is formed by the superposition of an upstream source and downstream sink (of equal strengths) located colinearly with the oncoming free stream. As in 2D flow, the source doublet is the limiting case as the source-sink separation distance (*2s*) approaches zero. Keeping source strength constant, a closed body of increasing fineness ratio results with increasing separation distance. The velocity potential of a source and sink located on the *x*-axis at $x=\pm s$ is

$$\varphi_m = \frac{m}{4\pi} \left\{ \frac{-1}{\left((x+s)^2 + \beta^2 r^2\right)^{\frac{1}{2}}} + \frac{1}{\left((x-s)^2 + \beta^2 r^2\right)^{\frac{1}{2}}} \right\} \tag{2.68}$$

where $r^2 = y^2 + z^2$. The streamwise velocity due to these singularities is given by

$$\frac{\partial \varphi}{\partial x} = \frac{m}{4\pi}\left\{\frac{x}{\left((x+s)^2+\beta^2 r^2\right)^{\frac{3}{2}}} - \frac{x}{\left((x-s)^2+\beta^2 r^2\right)^{\frac{3}{2}}}\right\} \tag{2.69}$$

Using $L_{ref} = \sqrt{BH}$ as the reference length for nondimensional co-ordinates ($\xi = x/\beta L_{ref}$, $\eta = y/L_{ref}$, $\zeta = z/L_{ref}$) and for the singularity half-distance ($\sigma = s/\beta L_{ref}$), the streamwise wall interference for a Rankine body of revolution on the centreline of a closed-wall rectangular test section is found by summing all the image potentials,

$$\varepsilon = \frac{A^{\frac{3}{2}}}{4\pi\beta^2}\frac{m}{U_\infty BH}\sum_{\substack{n=-\infty \\ \text{excluding} \\ n=m=0}}^{n=\infty}\sum_{m=-\infty}^{m=\infty}\left\{\frac{\xi+\sigma}{\left[(\xi+\sigma)^2+\left(\eta\sqrt{A}-mA\right)^2+\left(\zeta\sqrt{A}-n\right)^2\right]^{\frac{3}{2}}} - \frac{x-\sigma}{\left[(\xi-\sigma)^2+\left(\eta\sqrt{A}-mA\right)^2+\left(\zeta\sqrt{A}-n\right)^2\right]^{\frac{3}{2}}}\right\} \tag{2.70}$$

The longitudinal distribution of blockage interference along the centreline of the tunnel for several Rankine bodies having a maximum diameter ratio $t/L_{ref} = 0.1$ is shown in Figure 2.20.

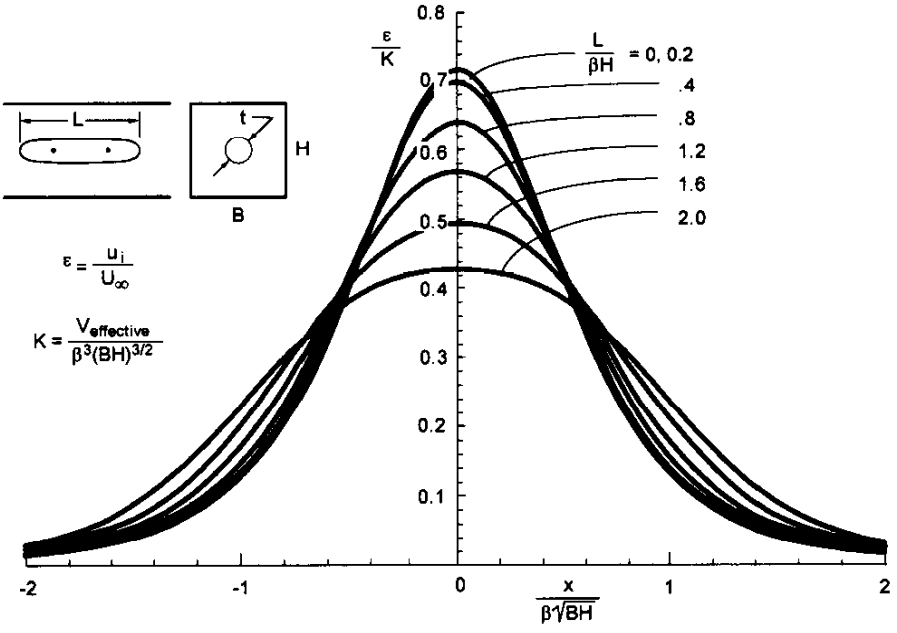

Figure 2.20 Streamwise Interference of Rankine Bodies
($t/\sqrt{BH}$ = 0.1) in a Closed-Wall Square Tunnel

The effect of large body length may be understood by considering the limiting case of a very long body. The flow between such a model and the walls is effectively 1D so that the interference at any station is approximately the velocity corresponding to the decrease in flow area due to the model cross section. By continuity,

$$(\rho UC)_{upstream} = \rho(x)\left(U_{upstream} + u_i(x)\right)\left(C - A_{model}(x)\right) \tag{2.71}$$

For small ε and A_{model}/C the blockage (to first order) at the centre (assuming the maximum body diameter occurs here) of a very long body is

$$\varepsilon = \left(\frac{A_{maximum}}{\beta^2 C} \right) \tag{2.72}$$

In AGARDograph 109 the effect of body length on peak interference is given for a Rankine body in a circular tunnel in terms of a modified tunnel shape factor. Figure 2.21 compares those results with similar calculations for Rankine bodies in a square tunnel. The square and circular tunnel results correspond very closely. The peak interference decreases significantly for model length ratios of practical interest. Typical large models may approach and even exceed length ratios of 1. Reflection plane models (so-called half-models) may approach length ratios of 2. The one-dimensional flow approximation is the interference asymptote for large model length and corresponds very closely to the 3D interference results for body length ratios above about 3. Results for a family of 2D Rankine ovals (*t/H=0.1*) are shown in Figure 2.21 for reference.

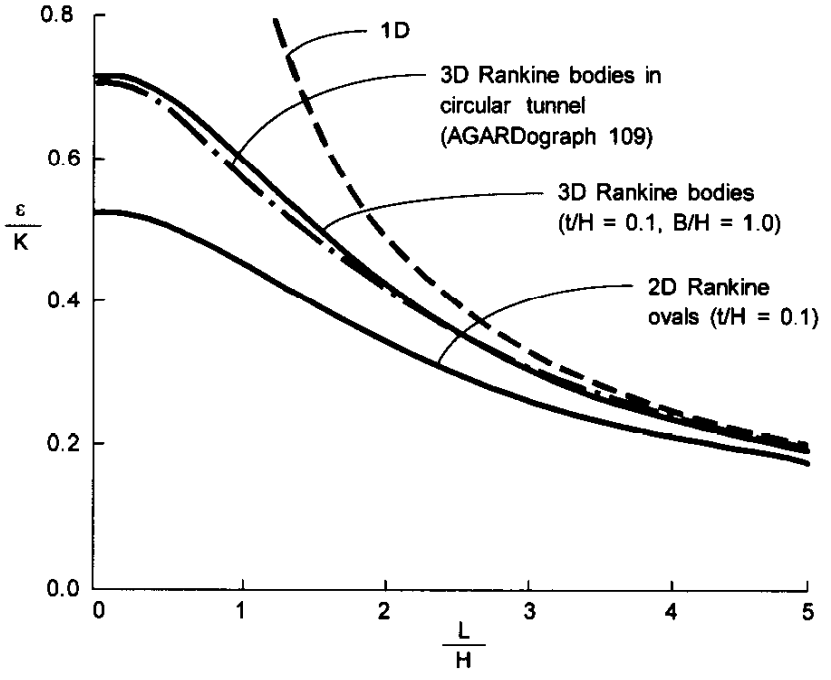

Figure 2.21 Effects of Body Length on Streamwise Interference

2.2.2.6 3D WAKE BLOCKAGE

In 3D flow, the potential of a point source is

$$\varphi_m = -\frac{m}{4\pi}\frac{1}{\left(x^2+\beta^2 r^2\right)^{\frac{1}{2}}} \tag{2.73}$$

where m, the source strength, is 1/2 U_∞ S C_D. The streamwise velocity due to this singularity is

$$u = \frac{\partial\varphi}{\partial x} = \frac{m}{4\pi}\frac{x}{\left(x^2+\beta^2 r^2\right)^{\frac{3}{2}}} \tag{2.74}$$

As in the previous section, a 2D doubly infinite array of image singularities (see Fig. 2.7) satisfies the boundary conditions for a rectangular closed-wall tunnel. Using $L_{ref} = \sqrt{BH}$ as the reference length for nondimensional co-ordinates ($\xi = x/\beta L_{ref}$, $\eta = y/L_{ref}$, $\zeta = z/L_{ref}$) as before, the nondimensionalised streamwise interference anywhere in the tunnel for a model located on the centreline of a rectangular tunnel is then given by

$$\varepsilon = \frac{A^{\frac{3}{2}}}{8\pi\beta^2}\frac{C_D S}{BH}\sum_{\substack{n=-\infty \\ \text{excluding} \\ n=m=0}}^{n=\infty}\sum_{m=-\infty}^{m=\infty}\frac{\xi}{\left[\xi^2+\left(\eta\sqrt{A}-mA\right)^2+\left(\zeta\sqrt{A}-n\right)^2\right]^{\frac{3}{2}}} \tag{2.75}$$

As for the 2D case, this formulation results in $\varepsilon = 0$ at the model location and a finite (negative) blockage far upstream of the model, Figure 2.22. The interference at the model location relative to the velocity far upstream is

$$\varepsilon_0 = \frac{C_D S}{4\beta^2 BH} \tag{2.76}$$

Along tunnel centreline ($\eta = \zeta = 0$) the buoyancy due to the longitudinal gradient of wake blockage is found (as for the 2D case) to be related to the solid blockage distribution,

$$\frac{\partial\varepsilon_{wake}}{\partial\xi} = \frac{C_D}{2}\frac{S(BH)^{1/2}}{V}\beta\varepsilon_{solid} \tag{2.77}$$

The relationship between the longitudinal gradient of wake blockage and the value of solid blockage is to be expected considering that the source doublet point singularity is the x-derivative of the velocity potential of a point source. Thus, the second derivative (with respect to x) of the velocity potential of a point source is the same as the first derivative (with respect to x) of a source doublet, except for the ratio of the respective singularity strengths. Because the image systems are identical for the wake and solid blockage cases, the interference flow fields will be related in this way.

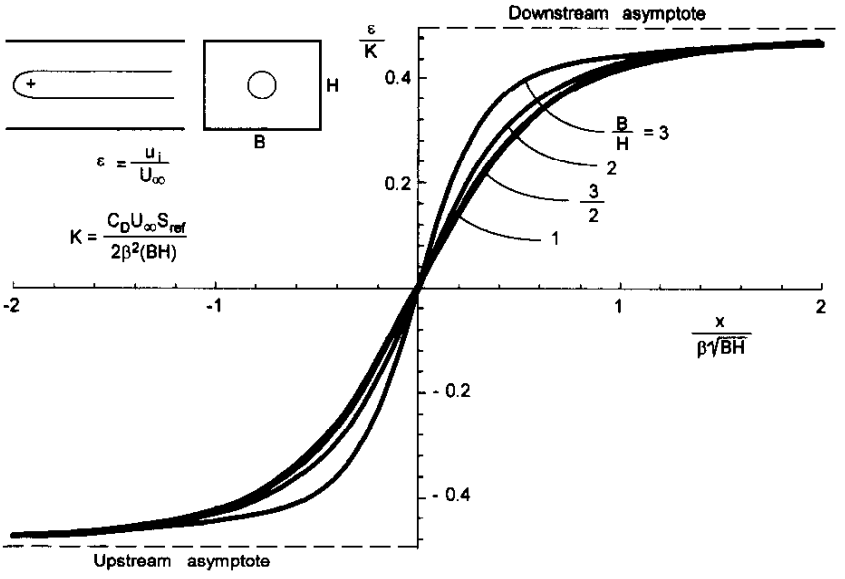

Figure 2.22 : Centreline Distribution of Streamwise Interference of a 3D Source in Closed-Wall Rectangular Tunnels

2.2.2.7 APPLICATION OF BLOCKAGE CORRECTIONS

The change of effective freestream magnitude at the model location necessitates correction of flow reference quantities: velocity, Mach number, dynamic pressure, static pressure, temperature, density, and Reynolds number. For small ε (taken to be the sum of all model elements contributing to blockage) and γ=ratio of specific heats=1.4, linearised corrections are as follows:

$$U_{corr} = U_{unc}(1+\varepsilon) \tag{2.78}$$

$$M_{corr} = M_{unc}\left[1+\left(1+0.2\,M_{unc}{}^2\right)\varepsilon\right] \tag{2.79}$$

$$q_{corr} = q_{unc}\left[1+\left(2-M_{unc}{}^2\right)\varepsilon\right] \tag{2.80}$$

$$p_{corr} = p_{unc}\left(1-1.4\,M_{unc}{}^2\varepsilon\right) \tag{2.81}$$

$$T_{corr} = T_{unc}\left(1-0.4\,M_{unc}{}^2\varepsilon\right) \tag{2.82}$$

$$\rho_{corr} = \rho_{unc}\left(1-M_{unc}{}^2\varepsilon\right) \tag{2.83}$$

$$\mathrm{Re}_{corr} = \mathrm{Re}_{unc}\left[1+\left(1-0.7\,M_{unc}{}^2\right)\varepsilon\right] \tag{2.84}$$

where the uncorrected flow parameters (subscript "*unc*") are identified with the remote upstream parameters (subscript "∞") in the tunnel.

For small models in a linear streamwise static pressure gradient, the pressure buoyancy force acting on the model in the tunnel is simply the product of the effective model volume and the gradient,

$$\Delta C_D = -\frac{V}{S\bar{c}} \frac{dC_p}{d\left(\frac{x}{\bar{c}}\right)} \cong \frac{2V}{S\bar{c}} \frac{\bar{c}}{\beta L_{ref}} \frac{\partial \varepsilon}{\partial \xi} \tag{2.85}$$

where $\xi = x/\beta L_{ref}$ and dC_p/dx is the externally imposed streamwise pressure gradient at the model location and, consistent with the perturbation assumptions, C_p is expressed as $-2u/U_\infty$. For a closed-wall tunnel, the measured drag of the model is increased, so that the necessary correction to drag is the negative of the above incremental buoyancy force.

For the 2D situation, the corresponding buoyancy drag force per unit span is

$$\Delta C_D = -\frac{A}{c^2} \frac{dC_p}{d\left(\frac{x}{c}\right)} \cong \frac{2A}{c^2} \frac{c}{\beta H} \frac{\partial \varepsilon}{\partial \xi} \tag{2.86}$$

where $\xi = x/\beta H$ and A is the effective cross-sectional area of the model.

2.2.3 Wake Blockage Corrections for Separated Flows

The problem of separated wakes, characterised by a free shear layer surface bounding a separation "bubble" behind the model, was recognised by Glauert [15], who accounted for the increased drag (attributed to blockage interference) due to separated wakes using an empirical factor η, which represents the size of the separated wake. Investigation of the effect of separated wakes was stimulated by the observed failure of classical interference theory for predicting tunnel constraints for flat plates at large incidence. The model that forms the theoretical basis for this correction is shown in Figure 2.23 (for 2D flow). For incompressible flow, Glauert's corrected dynamic pressure is

$$q_{corr} = q_{unc}\left[1 - \eta \frac{t}{H}\right]^{-2} \tag{2.87}$$

where t is the thickness of the blunt base. In three dimensions, t and H are replaced by the size of the separated wake at the body and C. For this case, Glauert quotes values of η as a function of t/c based on experiments with three Joukowski sections, a Rankine oval, ellipse, circle, and a flat plate.

Maskell [25] revisited the problem in trying to resolve differences in high-lift characteristics of delta wing models tested in different wind tunnels, especially beyond the onset of stall. For a flat plate normal to the

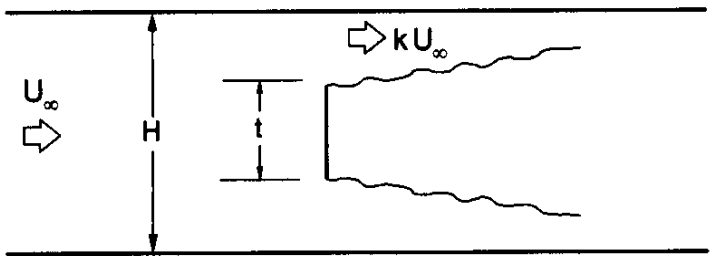

Figure 2.23 Model of Separated Wake Flow in a 2D Closed-Wall Tunnel

flow (similar to the situation of Fig. 2.23), the corrected dynamic pressure is derived as

$$q_{corr} = q_{unc}\left[1+\theta\frac{C_D S}{C}\right] \tag{2.88}$$

where θ, the blockage factor for bluff-body flow, is given by

$$\theta = \frac{1}{k_c^{\,2}-1} \tag{2.89}$$

The parameter k is related to the base pressure coefficient, C_{pb},

$$k^2 = 1-C_{pb} \cong k_c^{\,2}\left[1+\frac{C_D}{\left(k_c^{\,2}-1\right)}\frac{S}{C}\right] \tag{2.90}$$

and the subscript "c" refers to corrected quantities. Maskell suggests use of the iterative formula

$$\left(k_c^{\,2}\right)_n = k^2\left\{1+\frac{1}{\left[\left(k_c^{\,2}\right)_{n-1}-1\right]}\frac{C_D S}{C}\right\}^{-1} \tag{2.91}$$

to determine k_c, where subscript "n" denotes the nth estimate of k_c. For flat plates of aspect ratio between 1 and 10, a value of $\theta \cong 5/2$ is given as unlikely to result in serious error. This appears to be a consequence of the observed tendency of separated wakes behind rectangular flat plates toward axial symmetry. For this value of θ, the resulting blockage interference is five times greater (in terms of dynamic pressure correction) than if classical source-derived interference corrections were applied.

The extension of the above theory to a wing relies on the principle of superposition: it is supposed that the effect of the separated wake of the wing can be treated incrementally in a manner analogous to the normal flat plate. The most difficult part of determining this correction is evaluating the separated wake drag contribution. That is, the model drag can be considered to be the sum of three contributions,

$$C_{Dtotal} = C_{Dvortex} + C_{Dprofile} + C_{Dseparated} \tag{2.92}$$

where the first term is the inviscid induced drag due to lift, the second is the attached boundary layer profile drag, and only the third term is to be used in estimating the dynamic pressure correction due to separated wake blockage. Determination of the separated wake term requires determination of the onset of stall and a bookkeeping of profile drag and drag due to lift beyond stall.

2.3 PANEL METHODS FOR CLOSED-WALL TUNNELS

Advances in computational fluid dynamics (CFD) have paralleled the phenomenal increases in computational capability over the past 30 years. Even for simple model configurations in rectangular tunnels, it may be argued that solution of the boundary value problem with specified normal flow at control points at the wind tunnel wall is quicker and easier than calculation of the double summations of the previous sections. Continuing advances in computing power have put simple panel solutions within the capability of low-end engineering workstations and even personal computers.

With the maturation of production CFD codes and the development of custom wall interference codes, the calculation of wall interference for large models within test sections of arbitrary shape (including the effects of finite length) and with increasing accuracy with regard to the accounting of compressibility and viscous effects has been made possible and, in many applications, routine. Further, it is but a short step from the closed-wall boundary value problem to the ideal ventilated-wall boundary conditions (Sec. 3.2.3) and next, to use of measured wall boundary conditions (Chapter 4).

This section is limited to the application of CFD to wall interference for inviscid, linear compressible flows in closed-wall tunnels. As intended here, a "panel method" is any method in which the tunnel walls and, in many cases, the model are represented by singularity distributions on their surfaces. The singularities are fundamental solutions of Laplace's equation. Commonly used singularities include vortex lines for vortex lattice codes, constant strength source or doublet panels for simple panel codes, and higher order source or doublet panels for higher order panel codes.

The multitude of panel code applications to problems of wind tunnel interference precludes any attempt of an exhaustive review. In this regard AGARD R-692 [1] contains comprehensive review articles describing the wide range of interference problems and approaches in both Europe and North America. Although dated, this reference accurately reflects accomplishments and future directions of interference study in the premier aerospace laboratories of the participating countries. The problems identified at that time have since been pursued with ever more powerful computational tools. This section reviews some general principles of current CFD approaches, and provides a few examples that are indicative of typical results.

2.3.1 GENERAL CONSIDERATIONS

Evaluation of wind tunnel wall interference using a panel method provides advantages over classical methods based on the method of images with regard to both model and tunnel representation. First, the analysis of large and complex models is possible, though calculation of vortex wake trajectories and modelling of large separated wakes remain as areas of difficulty. Second, a panel approach to modelling the wind tunnel can directly address arbitrary cross-sectional shapes, streamwise variations of tunnel area, arbitrary wall boundary conditions (both in form and spatial variations), and the presence of support systems. The two main disadvantages (relative to simpler methods) are an increased complexity of analysis, involving more effort for preparation of analysis inputs, and the requirement for perhaps substantial computational resources.

A secondary disadvantage of panel solutions is the particular nature of each solution. That is, each flow condition (i.e., model configuration, position, attitude, and onset Mach number) requires separate analysis; generalisation of results is not immediately possible from a single analysis. Although in many cases linear theory may be used to establish typical parametric variations from the results of a single

solution for small changes of configuration or flow condition, a number of analysis cases may be needed both to verify classical trends and to capture variations of wall interference over the range of desired test variables (angle of attack, lift coefficient, Mach number).

The basic principles regarding the use of panel methods for interference calculation parallel those for the method of images. That is, the potential at any point in the flow is the sum of the potentials of all the panel singularities. The panel code solves for the strengths of all these singularities, subject to boundary conditions at each panel control point. The interference velocity potential of the walls is the sum of all the wall panel potentials. The wall panels thus produce the same incremental flow field as the entire collection of image singularities in the method of images. Zero interference around the model is obtained in the degenerate case of zero panel strengths everywhere on the wall. This will occur if closed-wall panels (with a $\partial\varphi/\partial n=0$ boundary condition) are disposed on an interference-free streamtube around the model. Alternatively, zero interference is obtained if the boundary conditions at each panel provide the interference-free velocity vector (i.e., due to the model alone), or simply if the walls are "far enough" away so that disturbances at the model due to the wall are negligible.

Figure 2.24, Vaucheret [35], provides model representation requirements in terms of wing geometry for a given error (0.03 deg/C_L) in interference upwash prediction for a square test section with closed sidewalls and porous floor and ceiling. This work indicates that a large range of sweep and span ratios are adequately represented by an infinitesimal horseshoe vortex ($2s/B=0$, $\Lambda=0$). Representation of finite wingspan captures a significant additional portion of the model wing design space, with wing sweep modelling required only for very large sweep or span ratio. Boundaries excluding models of large blockage and span ratios are also indicated.

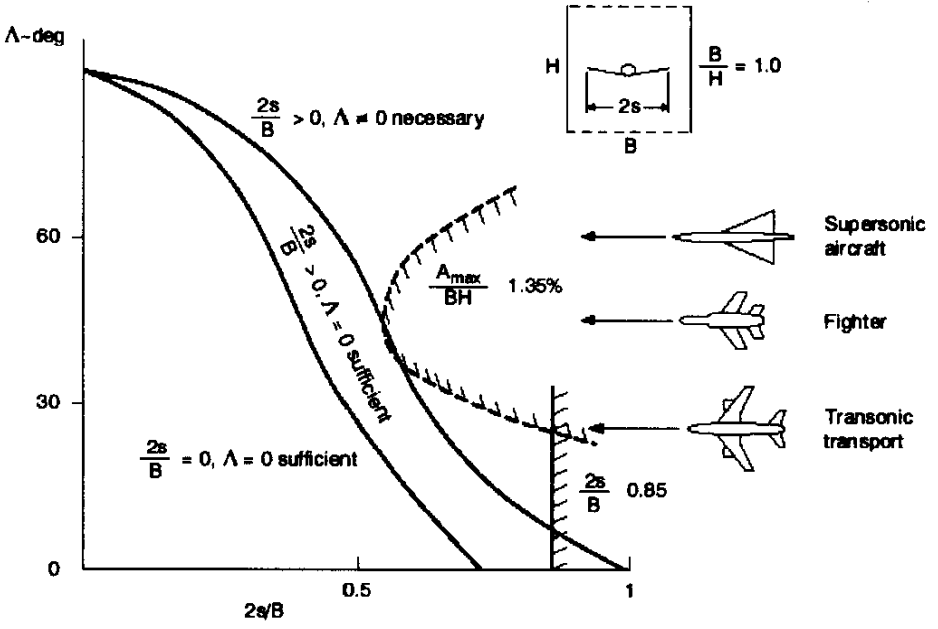

Figure 2.24 Modelling Requirements for Wings (Vaucheret [35])

Representations of the test model have increased in complexity concurrently with computational capability. The effects of finite model size can be represented by distributions of the fundamental model singularities within the test section. In general, any body shape can be generated by a distribution of source singularities. Similarly, any lift distribution can be approximated by a distribution of horseshoe vortex singularities. The strengths of these singularities are specified for a given flight condition.

Alternatively, model singularity strengths may be left as unknowns (requiring a corresponding set of boundary conditions or constraints), so that the effect of wall interference on model loading is explicitly calculated along with the interference field itself. Hybrid approaches are possible as well, wherein part of the model aerodynamics may be specified, such as the net source strength corresponding to skin friction drag.

For specified singularity methods, the model may be represented by a lumped parameter collection of singularities or singularity distributions that mimic the theoretical far-field interference-free flow around the model. To the extent that the distribution of singularity strengths represents the salient characteristics of the test article in the tunnel (volume distribution, lift, drag, pitching moment, span loading, etc.), this approach can be used to predict the interference of models that are not small. Complete image systems are usually not used explicitly. Rather, the tunnel walls are represented by a distribution of singularities located at the walls: source or doublet panels, or vortex lines, depending on the method. The closed-wall boundary condition ($\partial\varphi/\partial n=0$) is enforced at control points at the wall, resulting in a set of linear equations for the wall singularity strengths. The wall interference flow field is that part of the flow field due to the wall singularities only.

If the model is panelled, model panel strengths add to the number of unknowns subject to satisfying boundary conditions at the model surface. Leaving model aerodynamic loading as unknown is more exact than a priori specification of model aerodynamics, because satisfaction of the boundary conditions at the model includes the effect of the tunnel walls. In principle, this influence can include a change in separated wake shape if an appropriate wake model is implemented (Chapter 6). If model panelling is sufficiently dense, leaving model singularities as unknowns also permits the evaluation of interference from integrated model characteristics calculated both in the tunnel and in free air. Panel generation for straight, closed-wall tunnels with parallel walls is straightforward; panelling of the model, a variable-section tunnel, or a support system may require significant effort.

The issues facing an analyst using a panel method for wall interference prediction may be categorised as relating to:

1) Problem formulation: specification of boundary conditions may put the existence or uniqueness of a solution in jeopardy.

2) Tunnel panelling: tunnel length, circumferential and longitudinal panel density.

3) Model representation: number and distribution of singularities; panel density.

The computational approaches to wall interference calculation described here are in large part based on the use of flow codes developed for the analysis of so-called external flows. Their application to internal flows, such as the wall interference problem, usually involves embedding the tunnel in a uniform onset stream. As discussed by Holt and Hunt [19], using these methods to solve for the flow with both internal (the model) and external (the walls) boundaries cannot be done with impunity. Indiscriminate application of boundary conditions can result in uniqueness and existence problems for the sought-after solution. For example, a tunnel having closed and parallel walls may be modelled as a panelled prism with upstream and downstream faces normal to the tunnel axis. However, the normal flow on each of these faces cannot be independently specified. The panels representing the tunnel walls have a specified zero normal flow, so continuity of mass requires that integrated inflow to the tunnel must equal integrated outflow. Holt and Hunt address this problem by placing the wind tunnel, modelled as a long open-ended tube, in an external uniform flow field and parallel to it. Other variations on this approach may be code-dependent, but typically involve specification of flow at one end of the tunnel, either explicitly or implicitly.

Figure 2.25 summarises the boundary conditions for a wind tunnel analysis using a panel code similar to PANAIR (Magnus and Epton [24]).

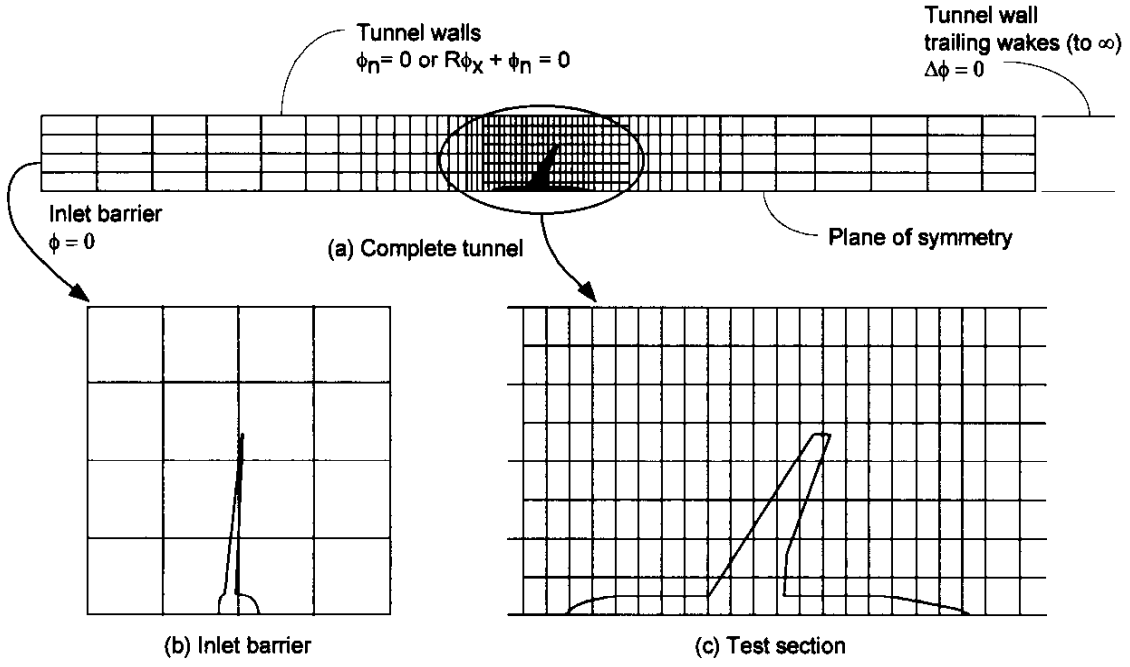

Figure 2.25 Boundary Conditions for a Tunnel Analysis Using PANAIR

Tunnel panelling should be guided by the usual common-sense panelling rules. Panelling should be dense enough to capture the flow features of interest. A simple check consists of increasing panel density until the solution stops changing. To represent the theoretical infinitely long tunnel, a panelled tunnel must be long enough that flow perturbations due to the model are negligible at the upstream end. Inspection of wall panel strengths and verification that they approach the desired zero upstream asymptote of the ideal long tunnel are recommended checks of any new solution. Evaluation of the uniformity of the incoming flow field at the upstream end of the tunnel is an additional check of the adequacy of upstream tunnel length. Downstream of the model similar considerations apply, though flow perturbations due to the model cannot be expected to disappear because of the convected model wakes (both vortex and viscous). However, the flow should approach an asymptotic state in the downstream direction as well. Again, inspection of wall singularity strengths or the flow field can indicate the adequacy of downstream tunnel length.

Similar considerations govern the specification of model singularities or panels. The safest approach is to increase model singularities (panels) until the calculated interference stops changing. If details such as changes in spanwise or chordwise wing loading are desired, model panelling must be as detailed as would be required of a free-air analysis.

Besides comparison of interference results from a panel method to classical results, other common-sense checks can lend credence to a particular panel solution. For closed-wall tunnels the walls should not leak: the massflow entering the tunnel at the upstream face plus any flow added at the model location should equal the massflow leaving the tunnel at its downstream end. Loss (or gain) of mass through the tunnel walls may be due to insufficient wall panel density, an error in panelling such as a reversed specification of panel normal vectors (conventionally, positive normal vectors point into the flow of

interest), or an improperly specified wall boundary condition. Another global "reasonableness" check of a closed-wall solution is the expected relationship of model lift to integrated pressure force on the walls: these should be equal and opposite. For ventilated walls similar considerations apply, but the momentum flux of the flow through the walls must also be included.

2.3.2 2D INTERFERENCE

Many advancements in wall interference technology were pioneered in the 2D domain due to its relative simplicity before similar techniques and approaches were applied to 3D flows. Analytic methods for 2D flows are more tractable; for example, complex variable techniques may be applied. For panel methods, the main advantage of 2D flows is computational simplicity due to greatly reduced problem size (i.e., number of unknowns). From the experimental standpoint, the primary advantage (for wall interference purposes) of the ideal 2D test set-up compared to a 3D test set-up derives from the fact that measurements and wall boundary adaptations are functions of only the streamwise co-ordinate. Thus both the number of measurements and the computational requirements to assess and reduce interference are typically at least an order of magnitude smaller than for a 3D test set-up.

Unfortunately, two factors conspire against the apparent simplicity of a 2D test: two-dimensionality of model disturbances and the model interaction with tunnel sidewall boundary layers. In two dimensions, flow disturbances due to a source doublet, for example, decrease as the square of the lateral distance from the model, compared to the cube of the lateral distance for a 3D doublet (see Sec. 2.2). Thus, the flow perturbations at the walls are larger for typical 2D cases than typical 3D cases, resulting in larger interference, and requiring the use of non-linear flow equations at much lower upstream Mach numbers. The sidewall boundary layer is more insidious because its response to the model pressure distribution can result in effectively a wavy sidewall, thus violating the required symmetry condition for planar flow. This issue is discussed in GARTEUR [14] and Mokry et al. [26]. Barnwell [6], Barnwell and Sewall [7] and Murthy [27], [28], [29] and [30] describe flow models for estimating the interference effects of the sidewall boundary layer.

Holt and Hunt [19] describe several applications of panel methods to wind tunnel interference problems. For 2D flows, a direct panelling approach was abandoned (due to "leakage" problems, unless a very dense panelling was used) in favour of a panel method using a standard Schwartz-Christoffel transformation. The airfoil has a 2-ft chord, a thickness ratio of 7%, and a chord-height ratio of 2/7. For 2D high-lift testing, it is shown that the lift curve of a clean airfoil is adequately corrected to interference-free conditions using classical corrections. With flaps deflected, however, classical corrections are shown to result in lift corrections 2-5 times greater than corrections deduced using a panel technique. In these calculations, leading-edge flap incidence was explicitly varied to match leading-edge pressure peaks to free-air calculations in order to produce an incidence scan at fixed flap angle.

2.3.3 3D LIFT INTERFERENCE

Joppa [20] describes a vortex lattice method for the calculation of upwash interference in closed-wall tunnels of arbitrary cross section, Figure 2.26. The walls are represented by a tubular vortex sheet composed of a network of square vortex rings. Results are shown for a uniformly loaded, finite-span horseshoe vortex centrally located in circular, square, and rectangular (B/H=5/3) tunnels. The longitudinal variation of interference essentially duplicates the result from the method of images for the square tunnel.

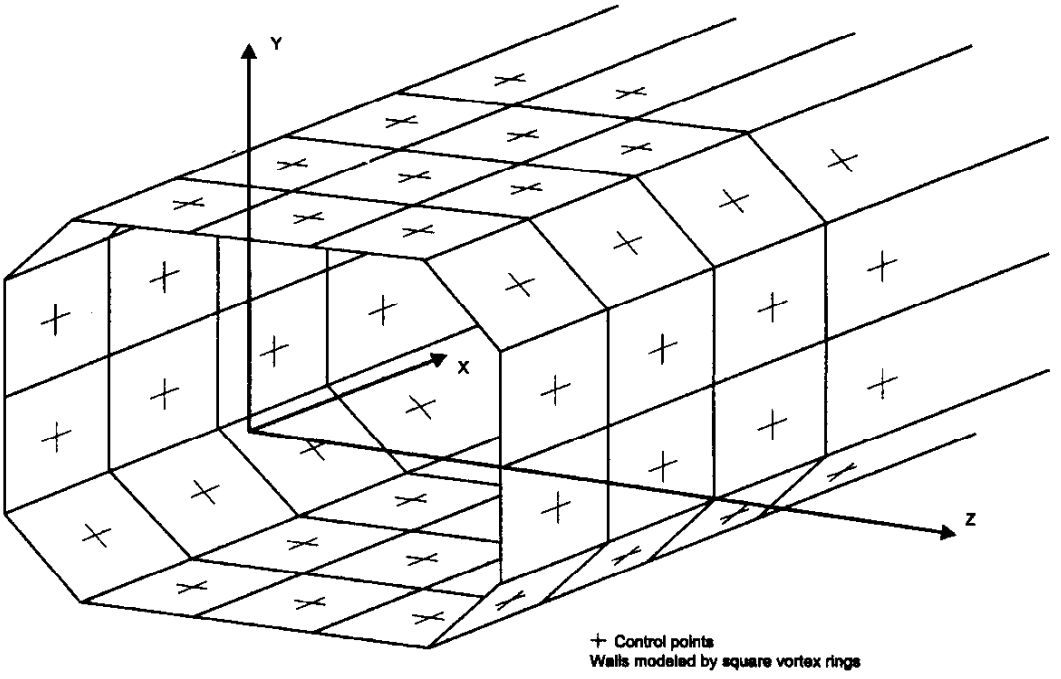

Figure 2.26 Vortex Lattice Representation of a Rectangular Tunnel with Corner Fillets (Joppa [20])

A panelling density consisting of 16 segments to represent the tunnel cross section was found to be adequate. Consideration of the longitudinal variation of calculated vortex strength at the walls suggests that the presence or absence of tunnel walls more than about a diameter upstream or downstream of the wing contributes little to the solution at the model. It is concluded that a length to diameter ratio of 3 to 4 is ample (for a vortex span ratio, $2s/B$=0.4). The method is used to calculate the upwash wall interference downstream of the wing, with stations above and below tunnel centreline representing typical tail locations (Joppa [21]). The effect of wake displacement was investigated and found to be significant with regard to upwash at the tail. It is concluded that wall-induced velocities cause the vortex wake to be deflected less than in free air, with the direct result that the upwash change at the tail due to the in-tunnel wake position may be of the same order as the usual wall interference upwash. This effect may be either positive or negative depending on tail location.

Holst [18] presents results comparing upwash variation as a function of wing sweep angle for constant and elliptic lift distributions using the method of Joppa [20]. Increasing root-to-tip upwash variation with increasing sweep angle, Figure 2.27, is expected given the longitudinal variation of upwash interference in closed-wall tunnels.

Holt and Hunt [19] give an example of a typical panel analysis of a tapered swept wing at 15 deg incidence of span ratio 2/3 in a rectangular tunnel. Their results illustrate both the effect of wall interference and of wake relaxation on span loading. The suppression of wake downward drift by closed wind tunnel walls is recognised as a potentially significant source of interference, especially for close-coupled configurations (e.g., canard-wing). It is noted that proper comparison of in-tunnel and free-air panel solutions to extract wall interference depends on consistent assumptions for the wake modelling. This work also illustrates a logical extension of the use of panel methods for wall interference evaluation: analysis of the complete testing environment including model supports.

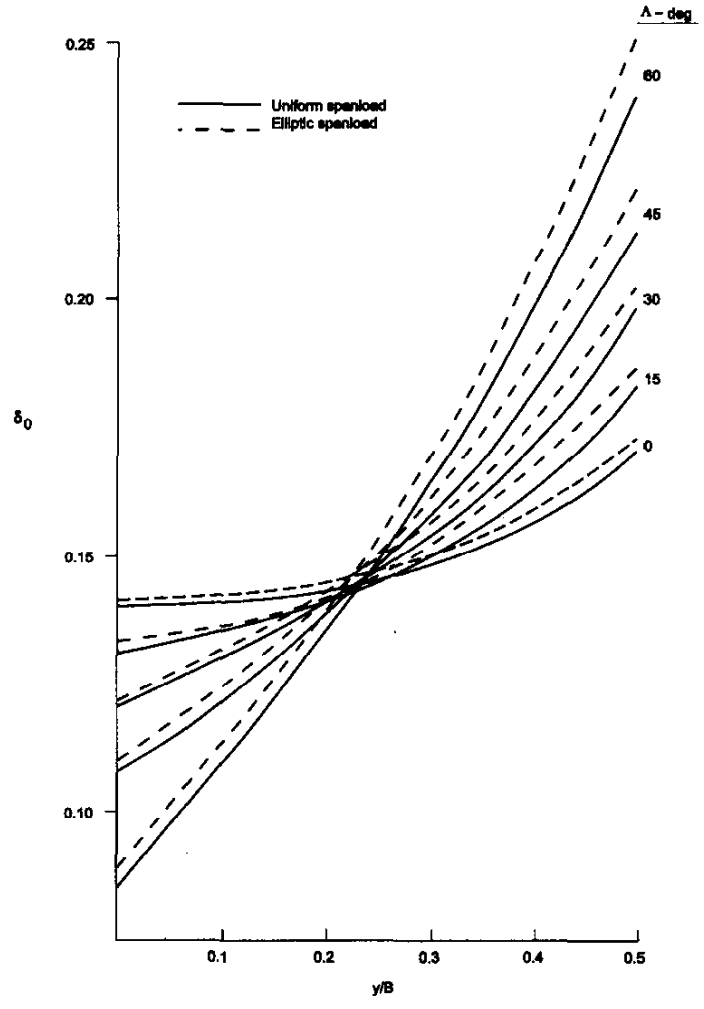

Figure 2.27 : Spanwise Variation of Upwash Interference for Swept Wing in a Closed-Wall Tunnel; 2s/B = 0,6, B/H = 1.0 (Holst [18])

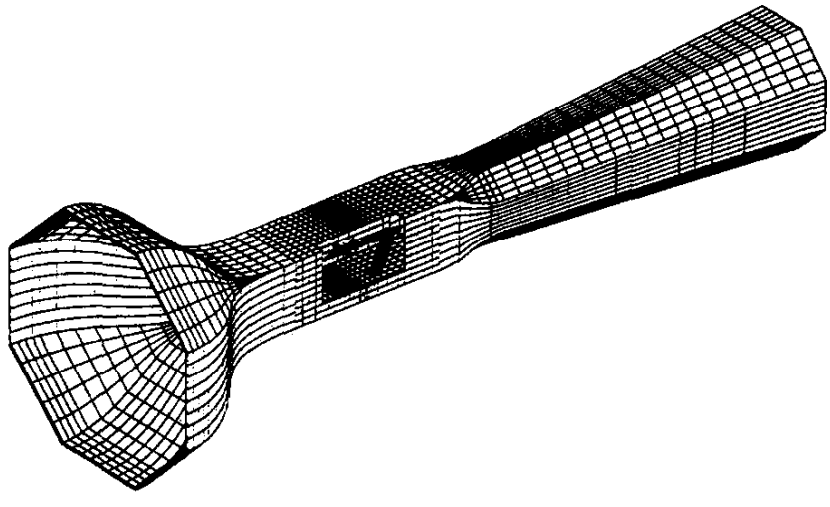

Figure 2.28 Complete KKK Wind Tunnel Panelling (Steinbach [33])

Steinbach [33] reports results of a panel analysis that further extends this approach in representing a complex test environment: the entire test leg, including aeroplane model and the sting support system, is panelled, Figure 2.28. The interference contributions of individual tunnel elements are compared. Calculated lift, drag, and pitching moment corrections due to the support system for a fighter model are found to be larger than corrections due to the walls.

With regard to experimental validation of a panel method for lift interference prediction, Vaucheret [36] compares incremental wall pressures due to model lift for the ONERA M2 model and demonstrates good agreement with predictions at an upstream Mach number of 0.81.

The interference of delta wings has been calculated using a free vortex sheet code (Frink [12]). The effects of span ratio and angle of attack are investigated. A dependence of lift interference on angle of attack is found and shown to be the result of the nonplanar vortex wake. The effects of tunnel walls on vortex sheet position and on upper surface pressures are also calculated.

A method exemplifying a hybrid of the method of images and panel methods is reported by Fiddes and Gaydon [11]. The test model and its first few images are panelled explicitly, permitting a relatively coarse wall panelling (Fig. 2.29). Engineering Sciences Data Unit Item 95014 provides upwash interference factors calculated using this method for a wide variety of wing planforms and span ratios in closed-wall rectangular tunnels. Chordwise and spanwise variation of the upwash interference factors, as well as average values, are given for wings of zero thickness centrally located in the tunnel. Cases include span ratios, $2s/B$=0.4, 0.6, and 0.8, for tunnel aspect ratios, B/H=10/7, 1, and 0.7.

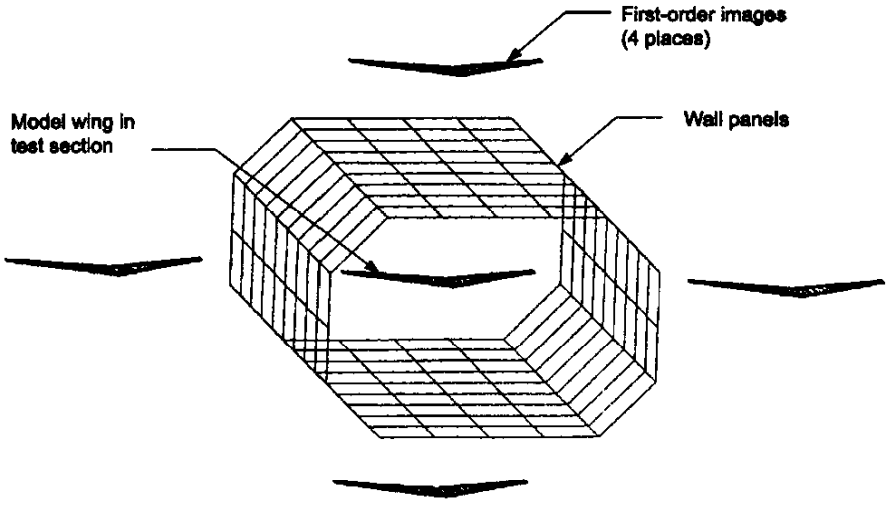

Figure 2.29 Hybrid Panel/Image Method (Fiddes and Gaydon [11])

2.3.4 3D Blockage Interference

Vaucheret [36] presents interference results using a multiple-singularity method whereby the adequacy of model representation is evaluated by inspection of wall pressures. A rule of thumb is proposed for ellipsoids: the number of source doublets should be at least twice the fineness ratio. Good correspondence of measured and predicted Mach number at the wall is shown for a missile configuration represented by 30 doublets. The effect of the model support sting is evaluated by additional doublets.

The adequacy of modelling is validated by comparison of experimental and predicted wall pressures (Fig. 2.30).

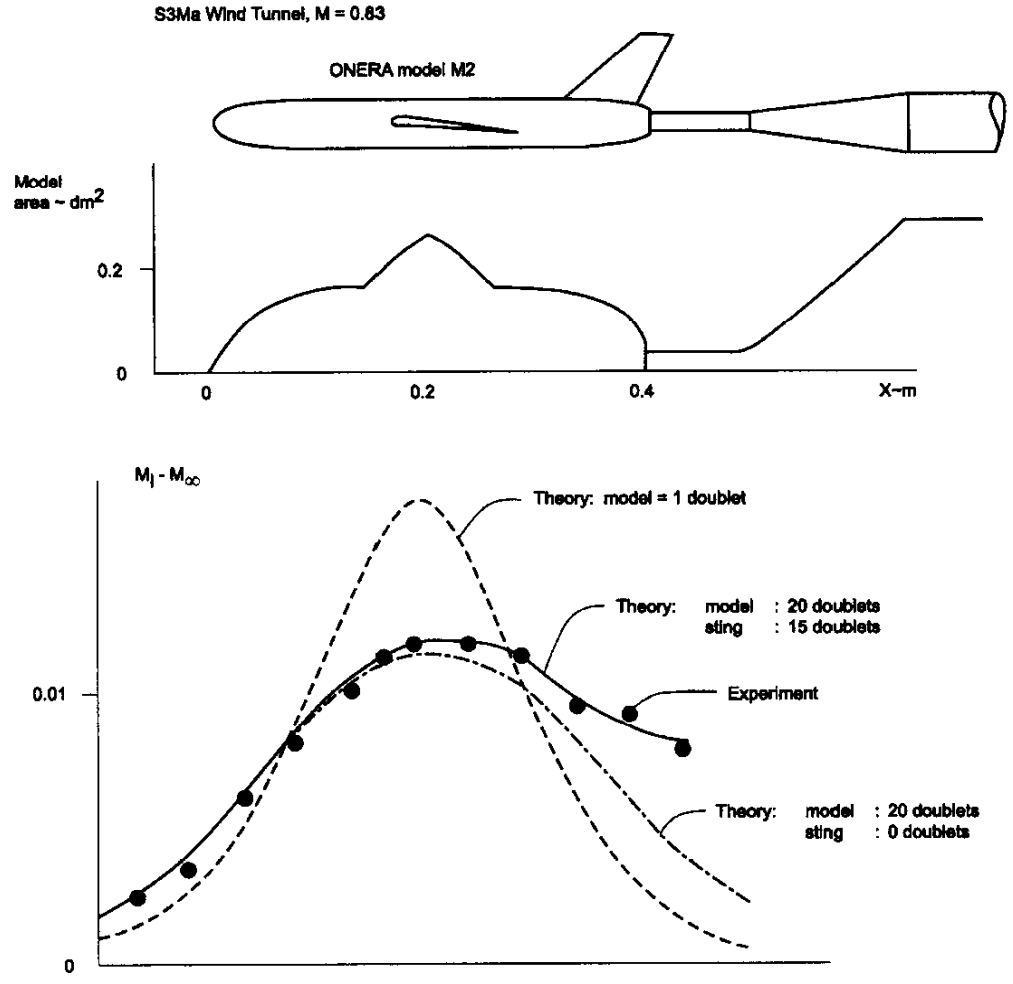

Figure 2.30 Wall Pressures due to Model and Sting in a Closed-Wall Tunnel (Vaucheret, [36])

Figure 2.31 shows the panelling of several axisymmetric bodies used as validation cases of a panel code calculation of wall interference. The maximum diameter of the bodies is about one-fifth the height of the tunnel. Figure 2.32 compares the results of blockage calculations for a Rankine body in rectangular closed-wall tunnels using a higher order panel code (Magnus and Epton [24]) to the method-of-images

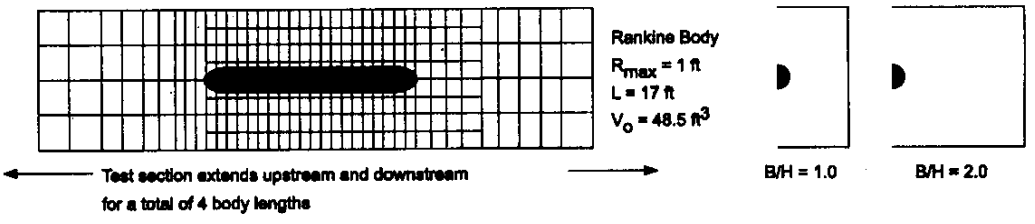

Figure 2.31 Rankine Body in Closed-Wall Rectangular Tunnels

calculations. Both the maximum value of interference and the distribution along tunnel centreline are essentially identical for these two methods. Interference predicted by classical methods for small models (Glauert, [15]) also agrees with these predictions if the finite-length body correction (Fig. 2.21) is applied to the Rankine body.

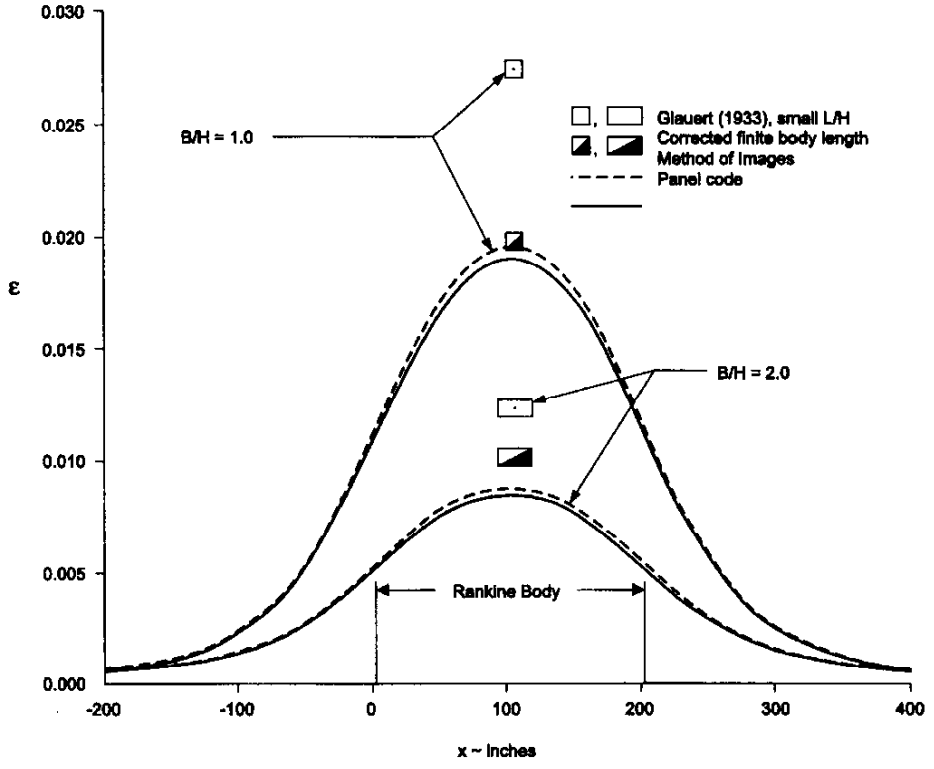

Figure 2.32 Blockage Interference of a Rankine Body in Rectangular Wind Tunnels, L/H = 1.5, M = 0

2.3.5 3D Wing-Body Combinations

The magnitude and importance of upwash wall corrections have served to focus many analysis efforts on the lift interference problem in isolation. Thus, factors bearing on upwash interference, span ratio, span loading, wing planform, and wake trajectory, have been reported extensively. The examples discussed in previous sections are representative but by no means exhaustive. Several citations also address lifting systems in combination with a blockage body and wake or sting system (e.g., Vaucheret and Vayssaire [35], and Vaucheret [36], are exemplary in discussing the spectrum of wall interference corrections in both closed-wall and ideal ventilated-wall tunnels).

High-lift testing of transport configurations is crucial for the development of multi-element high-lift systems. Lynch [23] gives an example of panel-code predictions of leading-edge slat pressure reductions due to the influence of closed wind tunnel walls. Because of the sensitivity of flow breakdown on the slat to this pressure minimum, wall interference can have a significant effect on maximum attainable lift.

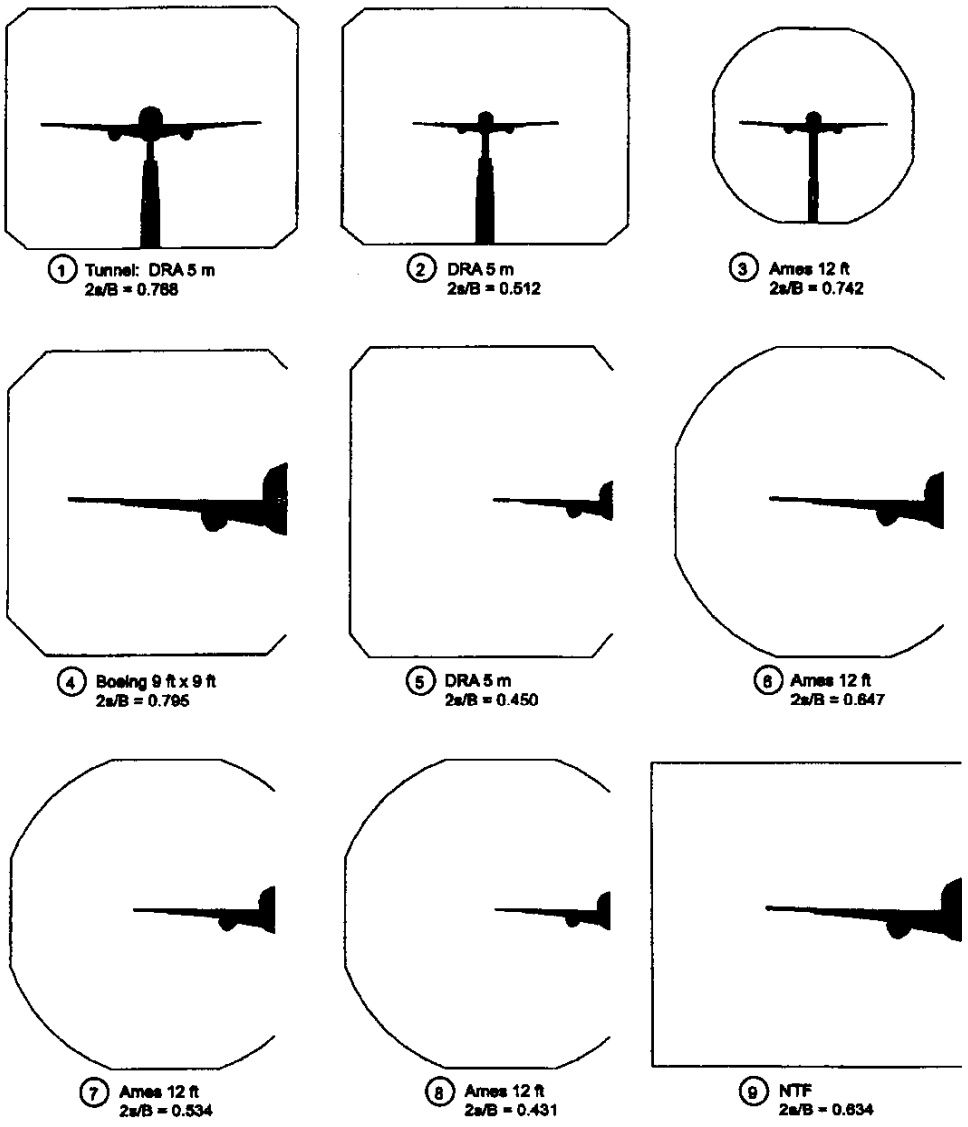

Figure 2.33 : Panel Study of Interference in Closed-Wall Tunnels (Amonlirdviman [4])

A similar computational study of high-lift transport configurations in closed-wall tunnels (Amonlirdviman [4]) Figure 2.33, quantified the spanwise interference variation at the wing for a variety of model-tunnel combinations. Both full and half-models were analysed. Full models were analysed with and without support strut fairings (shown in Fig. 2.33). Increased upwash and blockage interferences on the outboard wing are indicated for span ratios greater than 0.7, Figure 2.34.

A CFD study of a transport high-lift model in the Defence Research Agency (DRA) 5-meter, high-Reynolds-number wind tunnel was performed to validate the basic wall corrections used to reduce the wind tunnel data, to examine the spatial variation of the interference field, and to evaluate mounting system interference effects (Curtin [9]). The model is mounted at the tunnel centreline using a floor-mounted strut system and was analysed at two angles of attack, 6 and 15 deg. A side view of the panelling, Figure 2.35, shows the wing-body-nacelle model at 15 deg, the support strut, strut windshield,

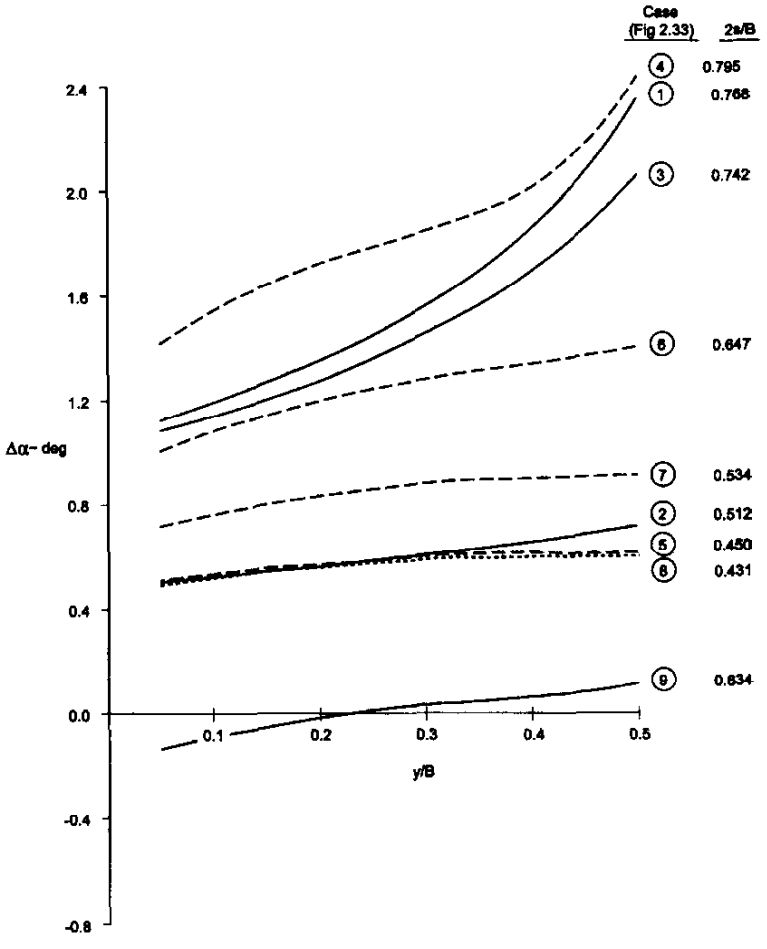

Figure 2.34 : Spanwise Variation of Upwash Interference (Amonlirdviman [4])

and floor and ceiling locations. The pitch link was not included in the panelling. The interference upwash angle and dynamic pressure ratio for a case with no mounting system, Figure 2.36, exhibit considerable variation over the wing planform. Upwash spans a range of over 1 deg from the leading edge of the wing root to the wingtip, with the tip at a higher angle of attack (therefore prone to premature stall in the tunnel relative to free air). The spanwise variation of blockage interference likewise increases the effective tip loading relative to free air. The span load in the tunnel reflects these effects, Figure 2.37. The interference velocity components, both streamwise and upwash, were evaluated at the 3/4 mean aerodynamic chord location. The streamwise interference velocity at this point was found to be different for the two angles of attack, with dynamic pressure ratios of 1.0093 and 1.0121, respectively. Using these values to compute model lift coefficient at each condition, the resulting lift interference parameter is δ_0=0.1394. These estimates compare to values of δ_0= 0.1463 and dynamic pressure ratio=1.0147 (independent of angle of attack) derived by classical means.

An example of the use of CFD to evaluate test section design concerns the effect of corner fillets on wall interference. The interference of a transport half-model in a proposed large low-speed tunnel was evaluated using a panel code, Figure 2.38. Interference at the model centre is reasonably represented by classical methods, Figure 2.39; even the incremental differences due to fillet size are qualitatively captured. Interference at the wing, Figure 2.40, shows significant deviation of interference from

centreline values, especially for the wingtip tip. Interference along an axial line through the mean aerodynamic chord is very similar to centreline values. Interference along an axial line near the wingtip reflects the calculated spanwise variation of interference.

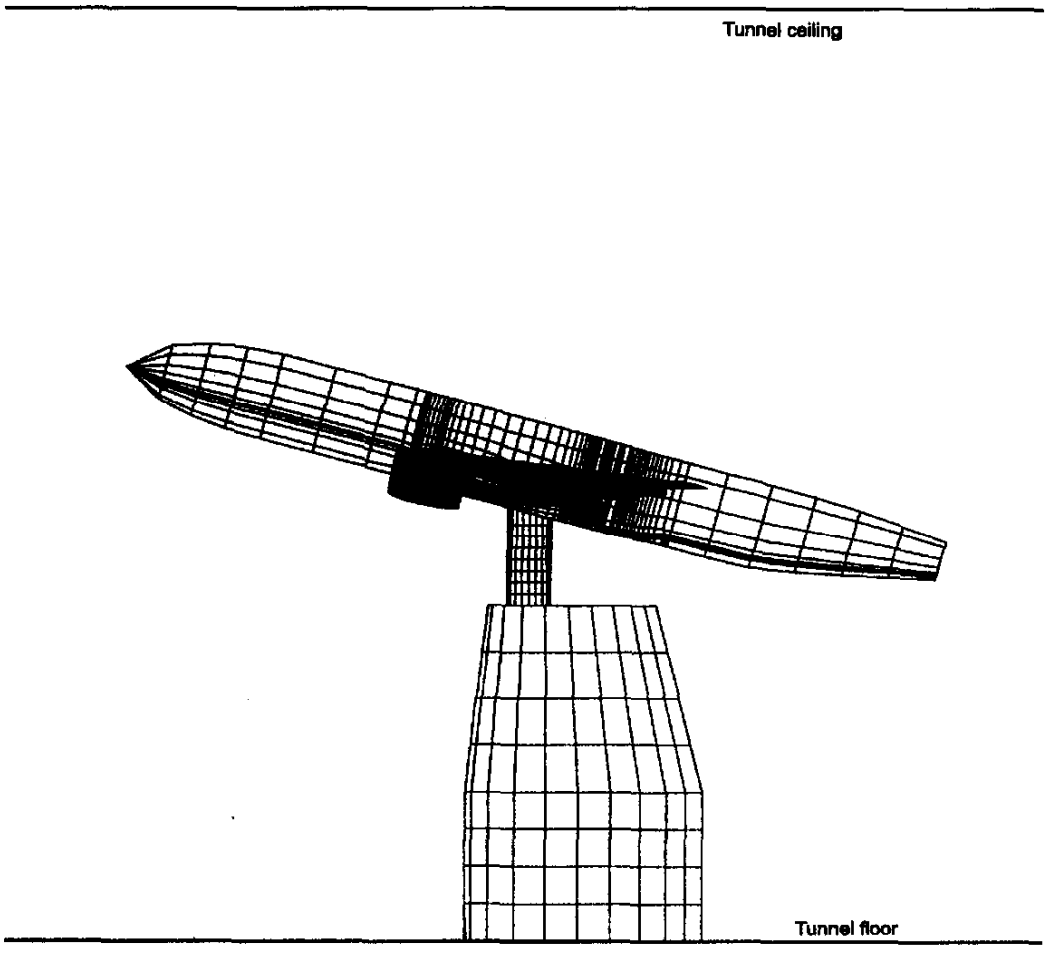

Figure 2.35 Panelling of Transport Model in DRA 5-m Wind Tunnel with Support Strut and Windshield (Curtin [9])

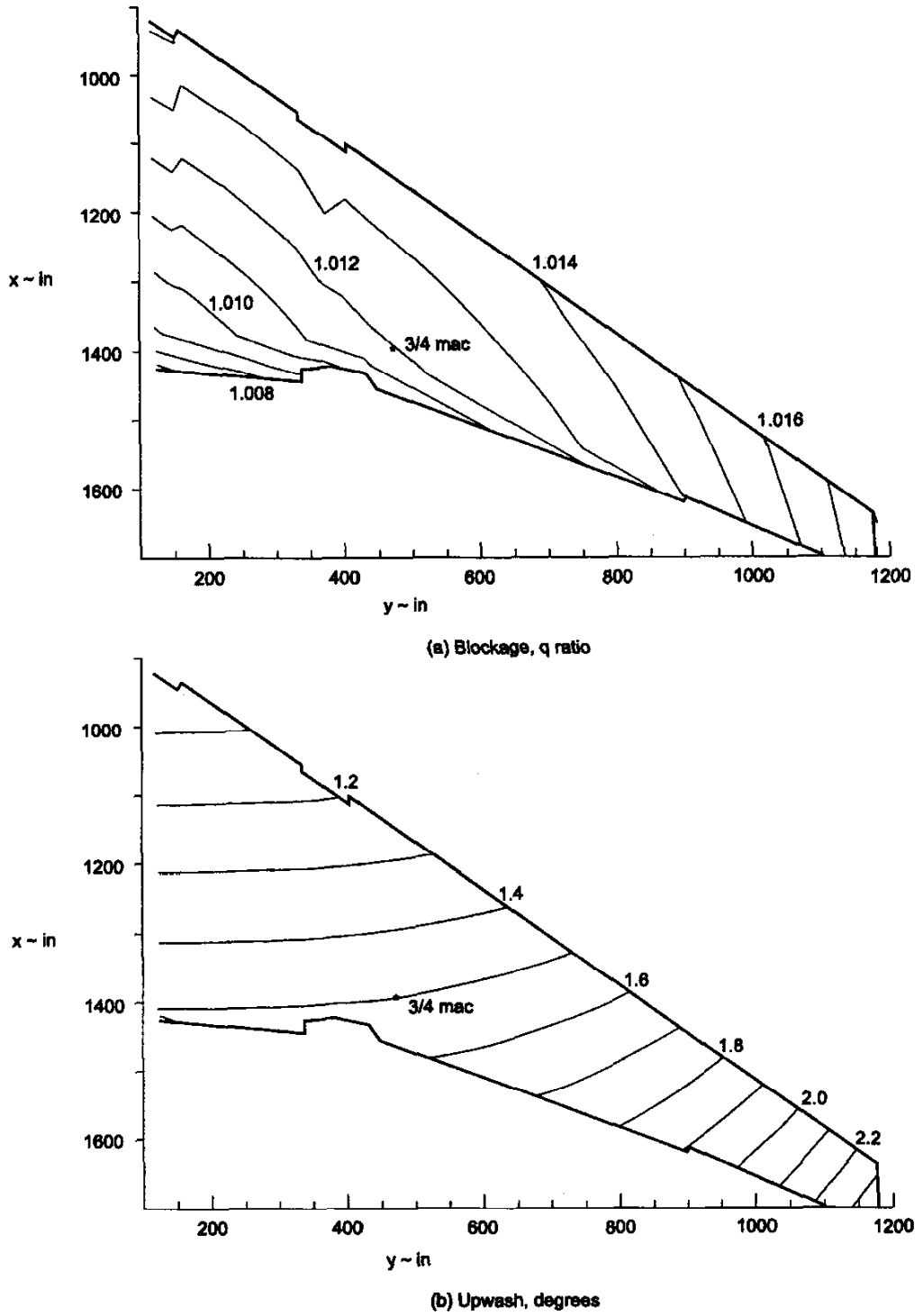

Figure 2.36 : Interference of Transport Model in DRA 5-m Wind Tunnel; $C_L \cong 2.3$, M=0.25, 2s/B=0.76 (Curtin [9])

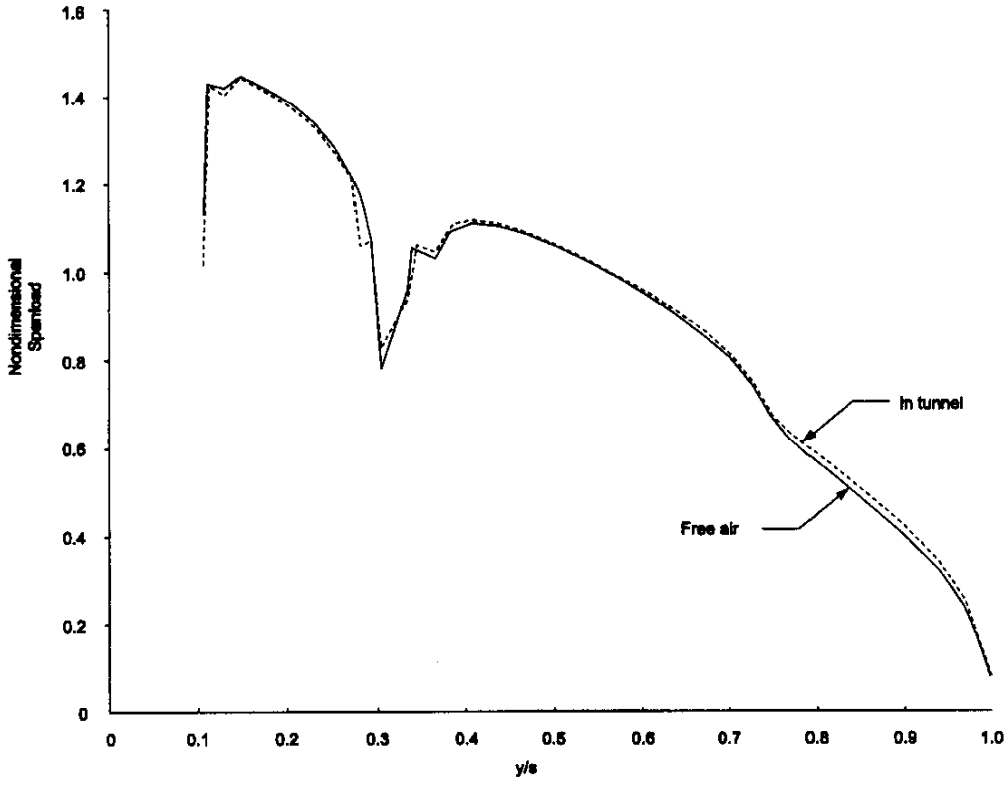

Figure 2.37 Span Load of Transport Model in DRA 5-m Wind Tunnel; $C_L \cong 2.3$, M=0.25, 2s/B=0.76 (Curtin [9])

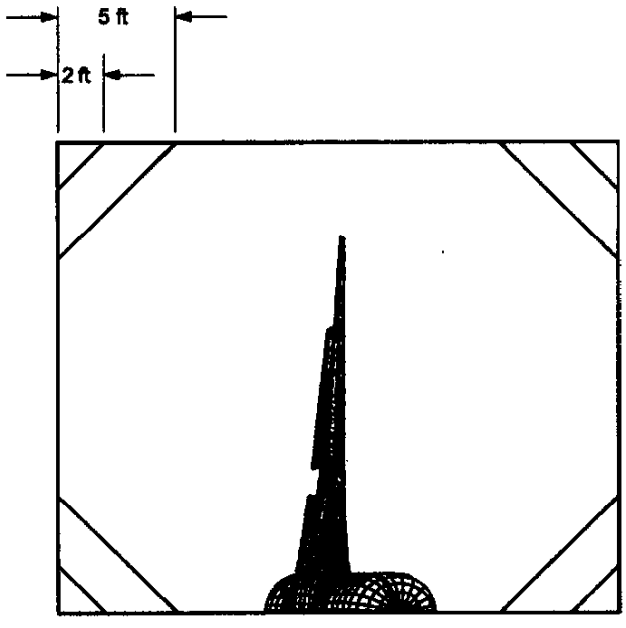

Figure 2.38 Low-Speed Wind Tunnel Corner Fillet Study; B = 40 ft, H = 24 ft

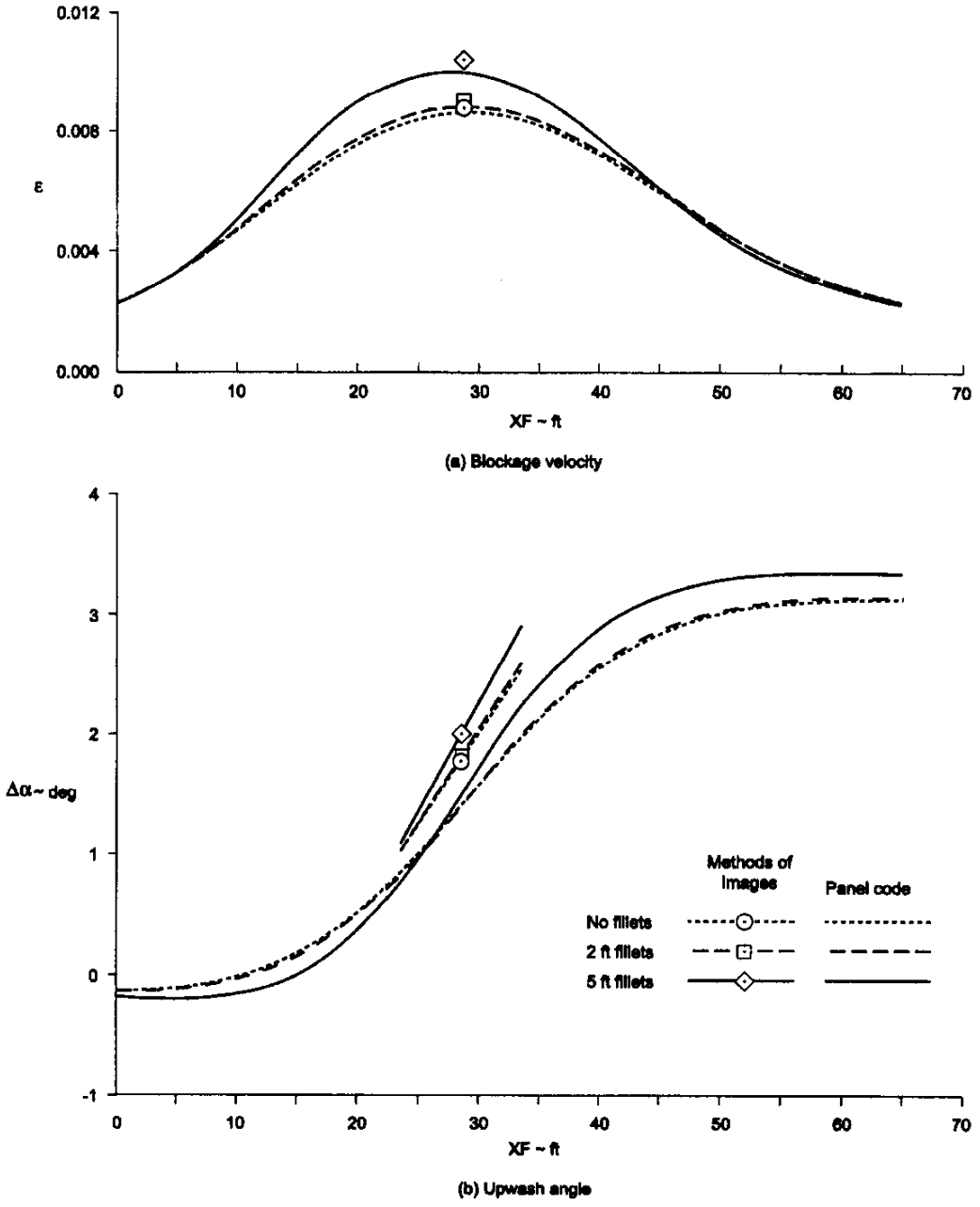

Figure 2.39 : Effect of Corner Fillets on Centreline Interference of a Subsonic Transport Model in a Closed-Wall Tunnel; B/H = 5/3, S = 129.43 ft^2, 2s/B = 0.8, C_L = 1.86

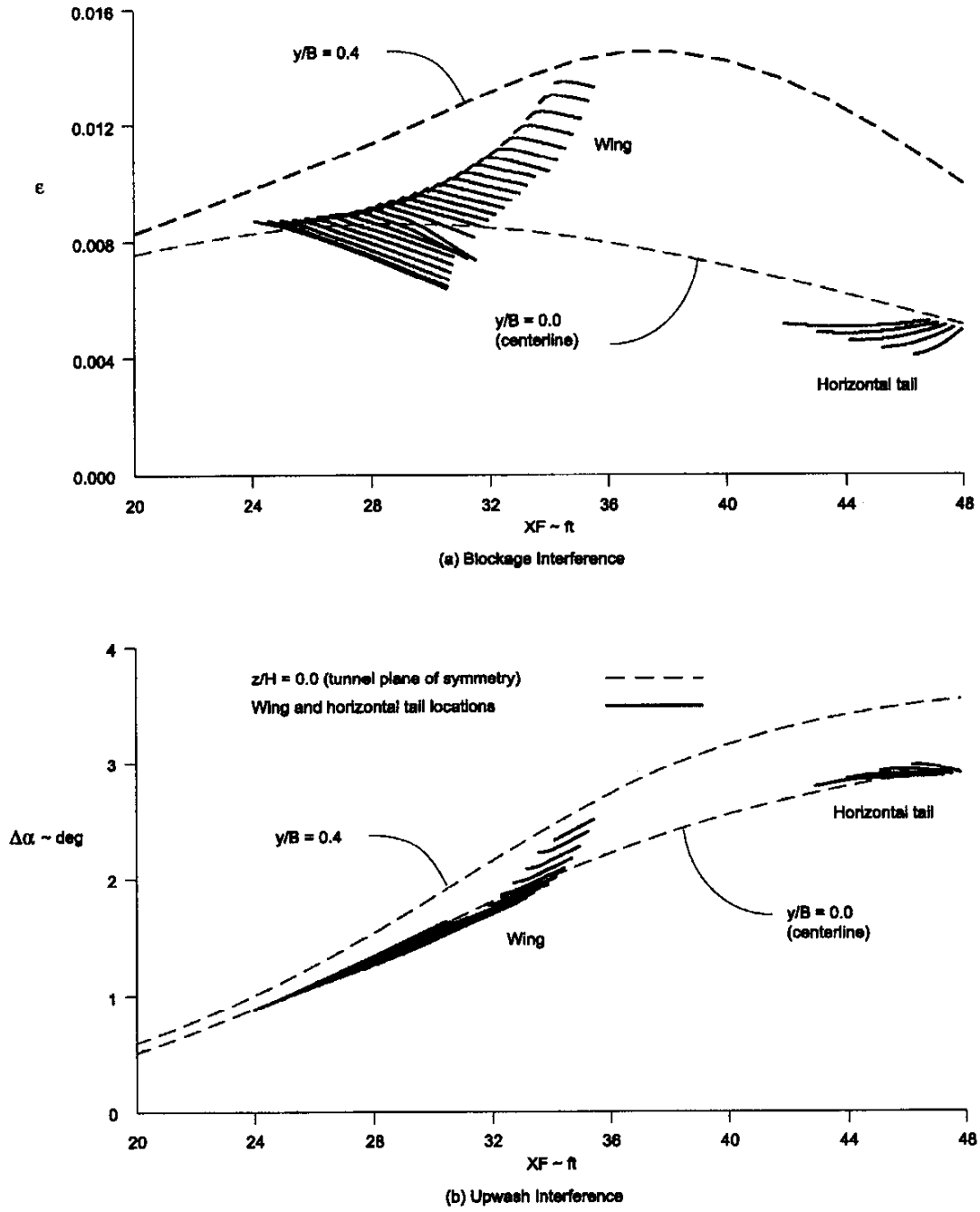

Figure 2.40 Wall Interference Variation at the Wing of a Subsonic Transport in a Closed-Wall Tunnel (No Corner Fillets); B/H = 5/3, S = 129.43 ft^2, 2s/B = 0.8, C_L = 1.86

2.3.6 SUMMARY OF PANEL METHODS

Panel methods for closed-wall tunnels have been used in a broad range of applications. Correspondence of wall interference from panel methods and classical methods has been demonstrated for small models. Unless extreme accuracy is required, classical methods are adequate for small models. The distribution of interference for large models (with no substantial separated flow) is credibly represented by panel methods at low subsonic Mach numbers, though in extreme cases the correctability of the flow field may be in question. The degree of correctability may be assessed by examination of the interference flow field. A computational approach for dealing with such issues has emerged as a force-correction method (Rueger et al. [32]) whereby CFD produces incremental corrections to model integrated forces and moments. To the extent that both the flow physics and the wall boundary conditions are accurately modelled, this approach can extend the correctability of model data beyond the boundaries of linear theory.

The use of panel methods to predict wall interference has in many cases supplanted classical techniques for closed-wall tunnels. The use of CFD for wall interference evaluation has further evolved along two parallel and complementary lines: more accurate specification of the wall boundary conditions and more accurate representation of the fluid physics. Wall boundary condition descriptions have moved toward one- and two-variable methods described in Chapter 4. Improved flow physics modelling includes the treatment of separated wakes (Chapter 6), vortex wake relaxation techniques, and the inclusion of compressibility in the flow equations for high-speed flows (Chapter 5). Such advanced methods are required for accurate interference predictions when these flow phenomena dominate the flow near a model that is "not small" relative to the tunnel. These methods are characterised by increased computational complexity and the requirement of measurements at the walls. Their use may also surrender the simplicity of the principle of superposition, a significant feature of linear potential flow. The success of panel methods over a wide range of subcritical flow conditions suggests their use not only in routine testing applications within their accepted range of validity, but also as a touchstone against which advanced methods may be tested.

2.4 CLASSICAL CORRECTIONS FOR OPEN TEST SECTIONS

2.4.1 INTRODUCTION

When Ludwig Prandtl started scientific aerodynamic work in wind tunnels about in 1915 at Göttingen, he designed his first wind tunnel with an open test section and a circular nozzle with 2.24 m exit diameter. Without doubt the open test section offers some advantages to the wind tunnel engineer. He enjoys the free accessibility to the test section flow, the easy installation of model suspensions and the simple installation of flow survey probes.

Nevertheless some twenty years later a different and more modern wind tunnel design standard was set mainly by Frank Wattendorf in the United States, which heavily influenced wind tunnel design all over the world. The closed test section was introduced. The advantage of a reduced power consumption, improved flow quality due to the smooth flow at the walls and a more precisely defined boundary condition of the test section flow, which made more precise wall corrections possible, outweighed the disadvantage of less comfortable accessibility. So today the closed wall test section dominates at least the aviation wind tunnel design. For a long time in Germany this was not the case. The authority of Ludwig Prandtl was so strong, that even the first low speed tunnels built in Germany after the war (and after the death of Ludwig Prandtl !) in about 1955 still were designed with open test sections.

For identical model dimensions generally the wall corrections are smaller (and have opposite sign) for open test sections than for closed wall test sections. Nevertheless the closed wall offers more precise wall corrections because of the more precise definition of the wall boundary condition.

Open test sections are still widely used in the automotive industry. The simple reason for the preference of the open test section is that automotive engineers prefer to test full scale cars instead of down-scaled models. Nevertheless for financial reasons these automotive tunnels are built too small at least according to the standards of aeronautical aerodynamicists. In a closed test section this size of „models" would result in severe flow field disturbance or even flow breakdown. The open test section is more forgiving and allows meaningful measurements even with blockage ratios, which are never used for aeronautical testing. In consequence the automotive engineers have a lot of trouble with wall corrections for large blockage ratios with bluff bodies, but this is not the general subject of this AGARDograph. For a more detailed analysis of bluff body corrections see chapter 6 of this AGARDograph.

In the recent past a new challenge in the wind tunnel technology brought the open test section back into the wind tunnel engineers' field of vision. Aeroacoustic testing becomes a more and more important part of low speed wind tunnels work load. At least at the moment the open test section, which shows no reflection of acoustic waves from the test section walls, is superior for aeroacoustic testing. It is easy, to equip the plenum around the open test section with sound-absorbing walls, which results in a very quite wind tunnel. Fortunately these aeroacoustic tests do not require ultra-precise wall corrections.

So the open test section wall corrections are less important at least for the aeronautical wind tunnel work and in this AGARDograph only a simple overview is given, which is more or less a condensed version of the open test section comments in the AGARDograph 109 [13].

In the wind tunnel literature sometimes the „¾ open wind tunnel" is mentioned. In most cases this term is used for automotive tests in open test sections with a closed floor, which represents the road. With respect to wall corrections the term „¾ open test section" is misleading. The closed floor of the test section is not a wall, which produces wall interference, but is part of the model configuration. So this test set-up is nothing else than an open test section. All formulas or methods for wall corrections can be

applied to this test set-up, if the total arrangement is reflected against the floor. The resulting test section with twice the height and two cars and a horizontal symmetry plane in the middle of the test section can be treated with normal open test section correction methods.

The basic principles of the classical wall corrections outlined in chapter 2.1 are valid for the closed test section and for the open test section as well. As mentioned already in chapter 2.1.3 the only difference is the wall boundary condition. The boundary condition of the closed wall is the non-existence of velocity components normal to the wall, which results in

$$\frac{\partial \varphi}{\partial n} = 0 \tag{2.93}$$

The boundary condition of the open test section is a constant pressure at the jet boundary, which corresponds to the static pressure of the plenum surrounding the test section. This boundary condition results in

$$\frac{\partial \varphi}{\partial x} = 0 \tag{2.94}$$

In the AGARDograph 109 some remarks and formulas are given for the corrections of two dimensional wings spanning open test jets. Since test set-ups like this totally disappeared from the aeronautical wind tunnel testing practice, this case is not mentioned here.

2.4.2 LIFT INTERFERENCE

The equations 2.27, 2.28 and 2.29 are valid for open test sections as well. According to the work of Theodorsen (1931) the result for the upwash interference is

$$\delta_o = \delta(0,0,0) = \frac{A}{8\pi} \sum_{\substack{n=-\infty \\ \text{excluding} \\ n=m=0}}^{n=\infty} \sum_{m=-\infty}^{m=\infty} (-1)^m \frac{m^2A^2 - n^2}{\left[m^2A^2 + n^2\right]^2} \tag{2.95}$$

The analogous expression for the upwash gradient at the model location becomes :

$$\delta_1(0,0,0) = \left.\frac{\partial \delta}{\partial (x/\beta H)}\right|_{0,0,0} = \frac{A}{8\pi} \sum_{\substack{n=-\infty \\ \text{excluding} \\ n=m=0}}^{n=\infty} \sum_{m=-\infty}^{m=\infty} (-1)^m \frac{m^2A^2 - 2n^2}{\left[m^2A^2 + n^2\right]^{\frac{5}{2}}} \tag{2.96}$$

The application of upwash corrections is described in section 2.2.1.4. The correction formulas are :

$$C_{Lcorr} = C_{Lunc}\cos\Delta\alpha - C_{Dunc}\sin\Delta\alpha \cong C_{Lunc} \tag{2.1}$$

$$C_{Dcorr} = C_{Dunc}\cos\Delta\alpha + C_{Lunc}\sin\Delta\alpha \cong C_{Dunc} + C_{Lunc}\Delta\alpha \tag{2.2}$$

$$\Delta\alpha = \delta_o \frac{S}{C} C_{Lunc} \tag{2.3}$$

The additional correction for the streamline curvature is given by equation 2.39 for the angle of attack :

$$\alpha_{corr} = \alpha_{unc} + \Delta\alpha + \Delta\alpha_{sc} = \alpha_{unc} + \left(\delta_o + \frac{\bar{c}}{2\beta H}\delta_1\right)\frac{SC_{Lunc}}{C} \tag{2.4}$$

and by equation 2.40 for the pitching moment :

$$\Delta C_M = \delta_1 \frac{\bar{c}}{16\beta H} \frac{SC_{Lunc}}{C} \frac{\partial C_L}{\partial \alpha} \tag{2.5}$$

Figure 2.41 [13] shows the lift interference on small wings in open and closed rectangular tunnels for comparison. In this figure the lift interference parameter is shown also for test sections with top and bottom wall only (type 3) and for test sections with side walls only (type 4). Such test sections are no longer used in wind tunnel practice.

For wings with finite span the lift interference parameter δ is given in Figure 2.42 [1]. These data are valid for uniform spanwise loading of the wings. The lift interference parameter is plotted against the „Effective span/Tunnel width" ratio; the parameter λ is the „height/width" ratio of the open test section.

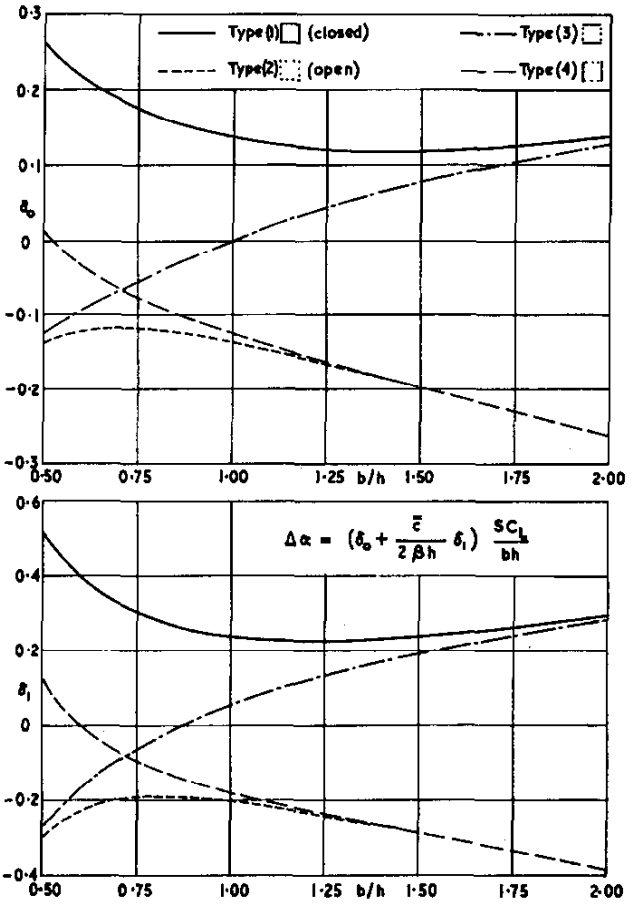

Figure 2.41 : Lift interference on small wings in rectangular tunnels

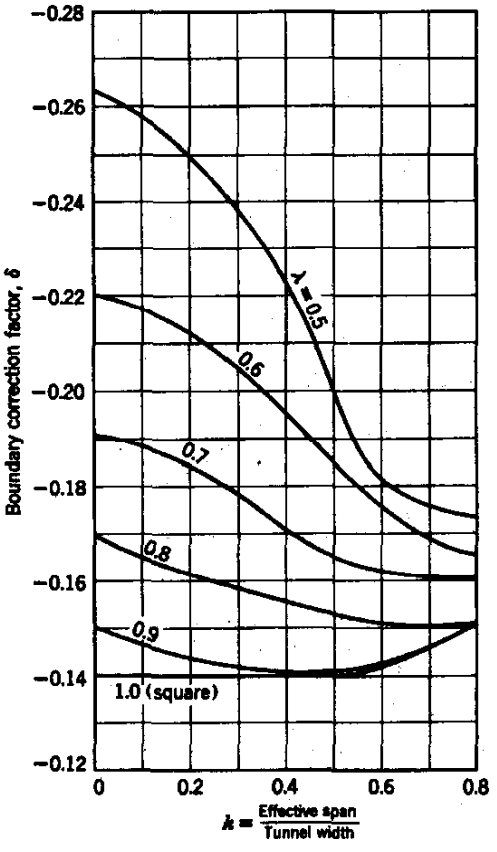

Figure 2.42 : Values for δ for a wing with uniform loading in an open rectangular jet

If the wing is displaced above or below the centreline of an open test section, the lift interference parameter may be taken from Figures 2.43 and 2.44. Figure 2.43 is valid for a square jet. Figure 2.44 gives the lift interference parameter for an open test section with a height to width ratio of 0.5.

[1] The Figures 2.42 to 2.50 were taken from [31]

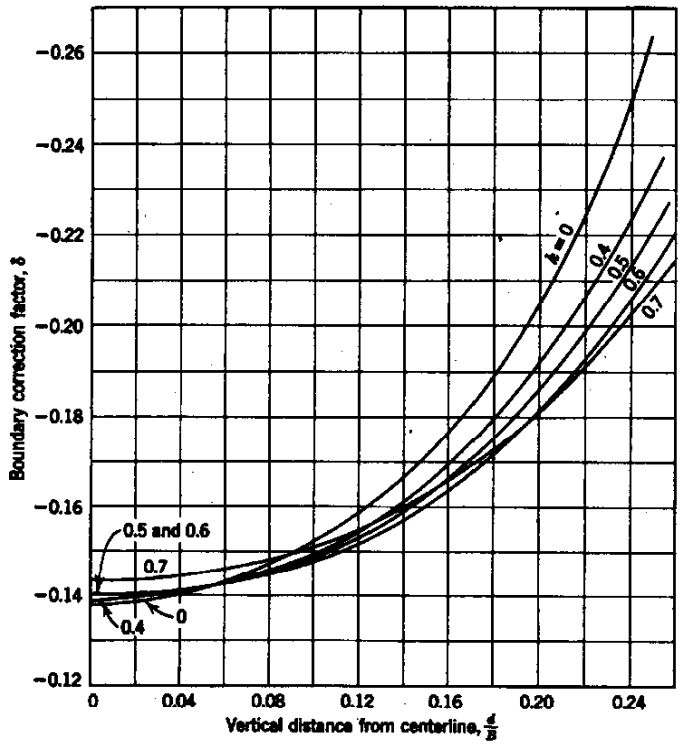

Figure 2.43 : Lift interference parameter for wings displaced above or below the test section centreline. (Square jet)

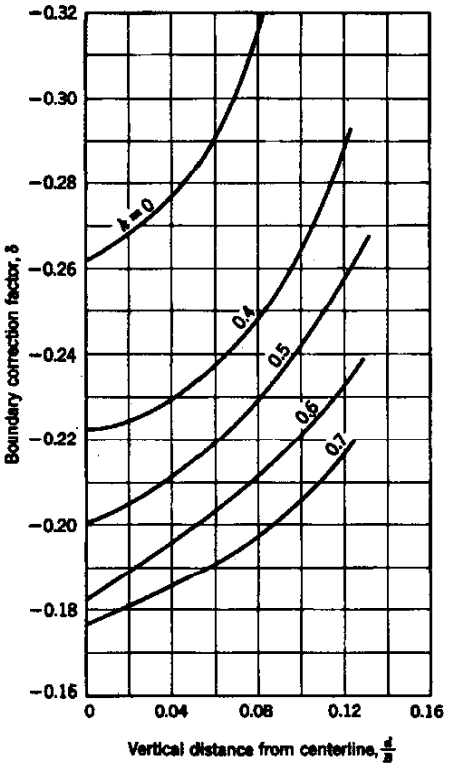

Figure 2.44 : Lift interference parameter for wings displaced above or below the tunnel centreline. Rectangular jet, λ = 0.5

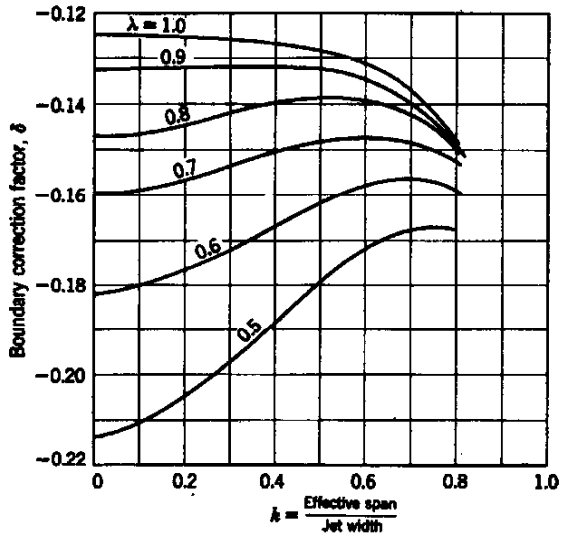

Figure 2.45 : Lift interference parameter for a wing with uniform loading in an open elliptical test section

A limited number of old wind tunnels with open circular or elliptic test sections are still in operation. For wings on the tunnel centreline with uniform loading Figure 2.45 gives the lift interference parameter for this test section configuration. In this figure the parameter λ = 1.0 designates a circular jet.

Figure 2.46 gives the lift interference parameter for elliptic open test sections with a width/height ratio of 2 : 1 for wings with uniform loading displaced from the centreline of the test section. Finally Figure 2.47 gives the lift interference parameter for wings with elliptic loading in circular and elliptic open test sections.

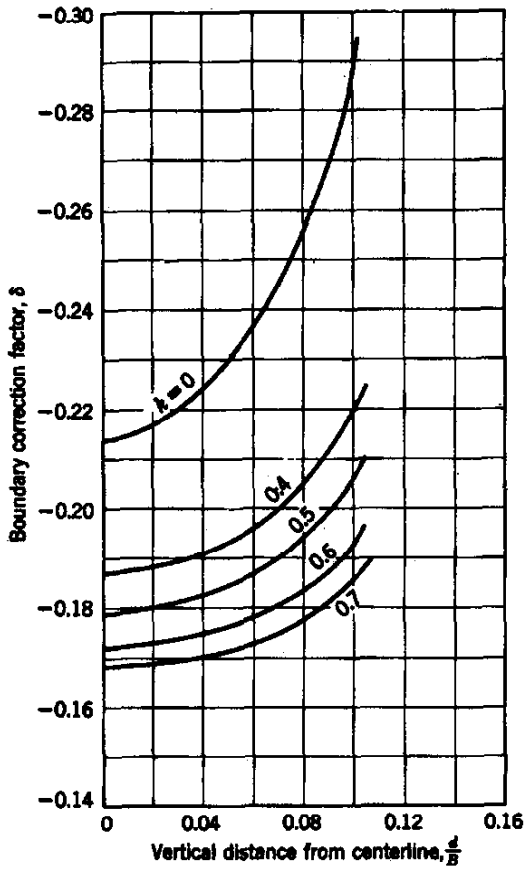

Figure 2.46 : Lift interference parameter for a wing with uniform loading displaced from the centreline of an open 2 : 1 elliptic test section.

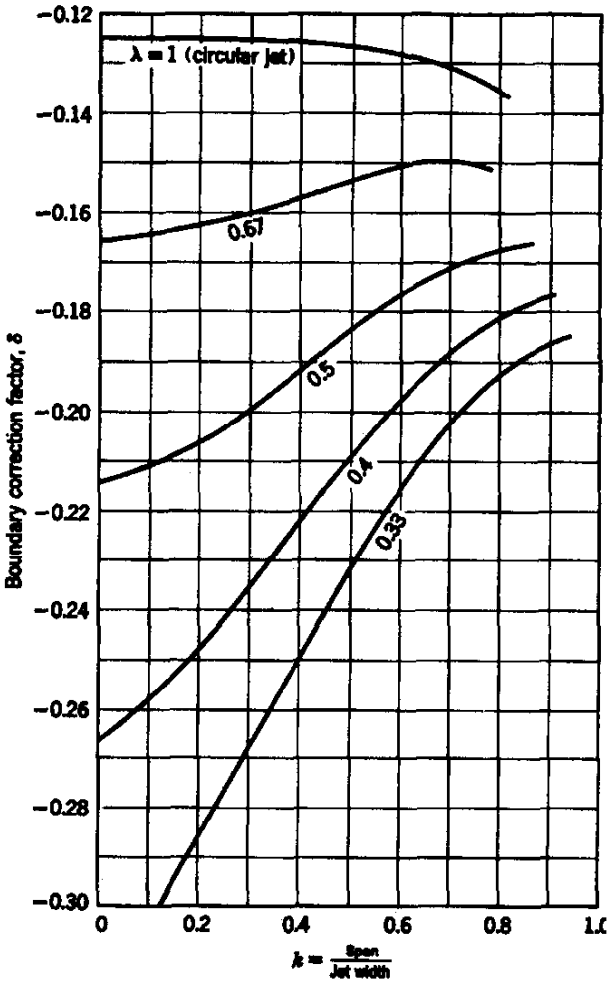

Figure 2.47 : Lift interference parameter for wings with elliptic loading in open circular/elliptic test sections

For the downwash correction at the tail of a model an additional correction factor τ_2 can be defined. At a distance l_t behind the quarter-chord line of the wing the boundary induced downwash w_k is :

$$w_k = \delta \frac{S}{C} C_{LW} (1 + \tau_2) V \tag{2.97}$$

For open test sections, some doubts exist about the validity of this correction if the tail length of the model is more than 40 % of the test section width.

Values for the downwash correction factor τ_2 are given in the Figures 2.48 to 2.51.

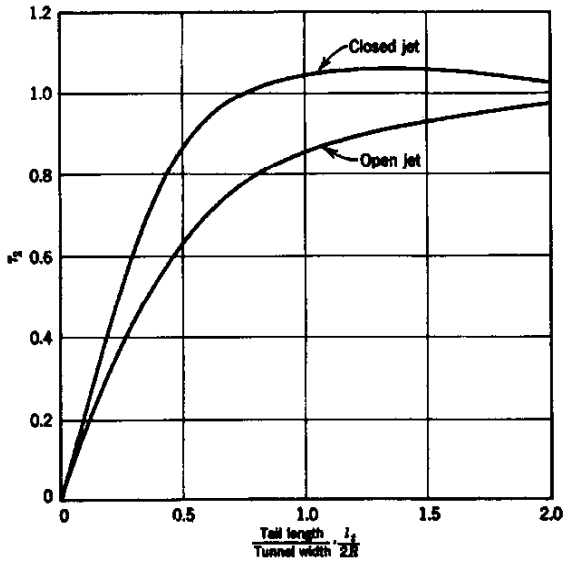

Figure 2.48 : Correction factor τ_2 for open and closed circular test sections

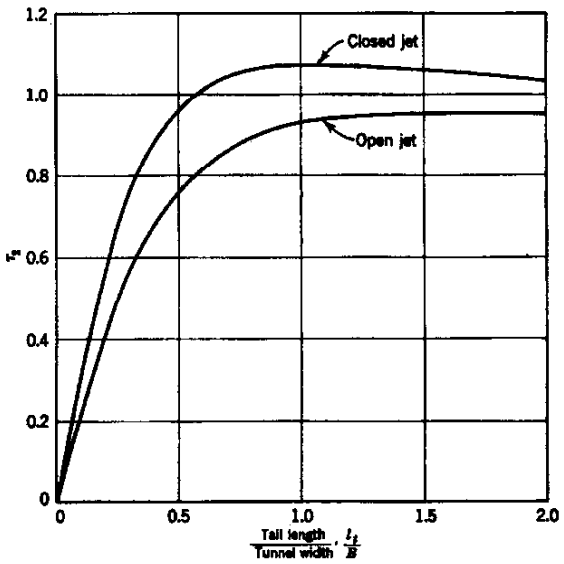

Figure 2.49 : Correction factor τ_2 for open and closed elliptic test sections

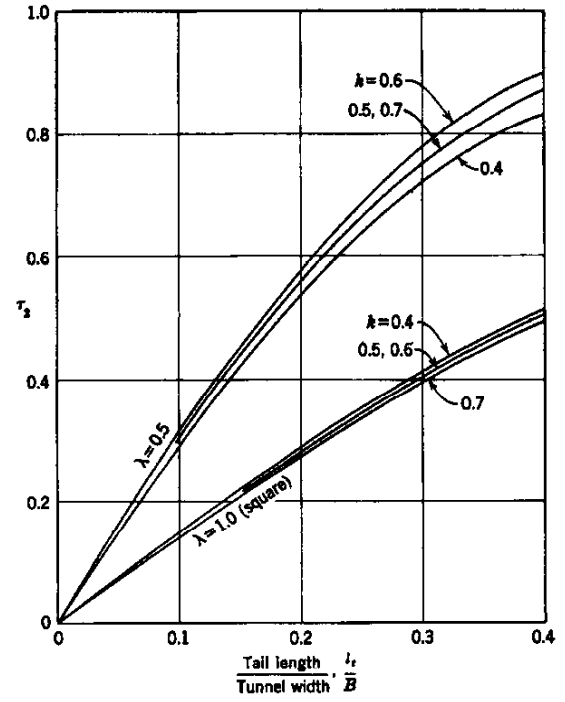

Figure 2.50 : Correction factor τ_2 for two open rectangular test sections, wing on centreline, tail on centreline

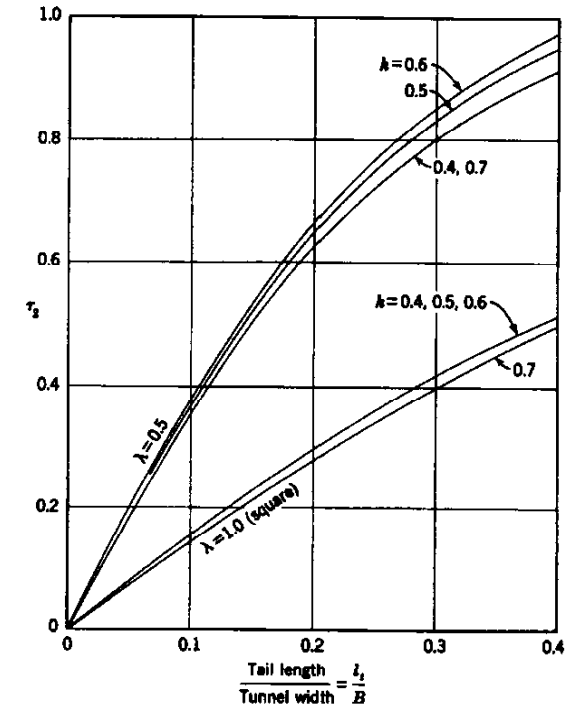

Figure 2.51 : Correction factor τ_2 for two open rectangular test sections, wing on centreline, but tail 0.1 b above or below centreline

2.4.3 BLOCKAGE CORRECTION

As for a closed tunnel, the boundary condition of a small model at the centre of a square open jet can be represented by an infinite set of images. In this case the signs of the doublets alternate, so the interference velocity at the models position is smaller than in the case of closed walls and of opposite sign. For the square open test section case in [13] (after Lock [23]) equation (2.98) is given, which in terms of model volume and with allowance for compressibility effects results in the simple equation (2.99).

$$\varepsilon_S = \tau\left(\frac{A_m}{h^2}\right)^{3/2}\lambda_3 \tag{2.98}$$

$$\varepsilon_S = -0.211\frac{V}{\beta^3 h^3} \tag{2.99}$$

For rectangular open test sections Wuest [37] evaluated values for τ :

$$\tau = \frac{1}{2\pi^{3/2}}\sum_{-\infty}^{\infty}\sum(-1)^{m+n}\left(\frac{bh}{m^2b^2+n^2h^2}\right)^{3/2} \tag{2.100}$$

The results are plotted in Figure 2.52[1].

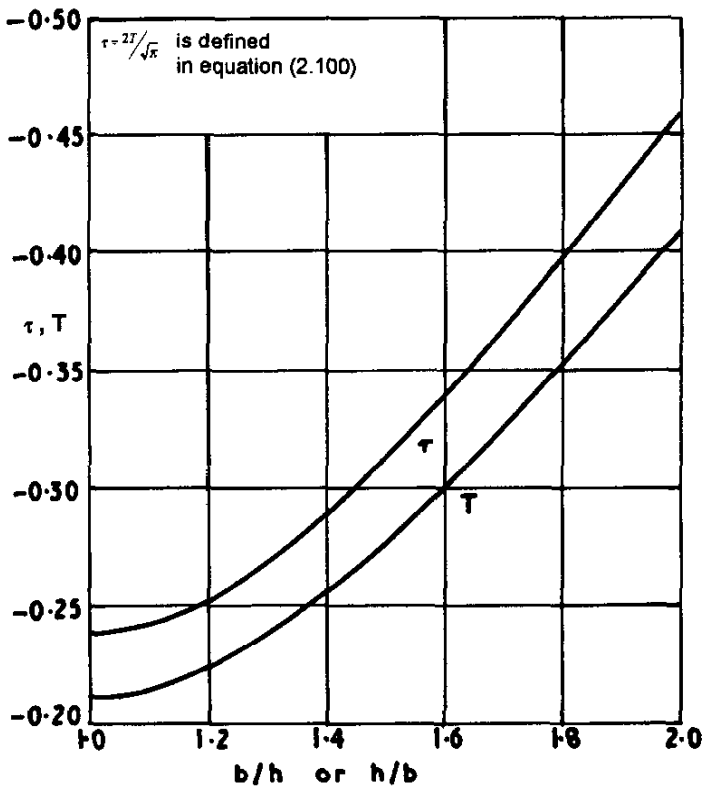

Figure 2.52 : Tunnel-shape parameters for small models in open rectangular tunnels

[1] The Figures 2.52 and 2.53 are taken from [13]

For circular open test sections Lock [22] gave an equation

$$\varepsilon_S = -0.206\left(\frac{A_m}{C}\right)^{3/2}\lambda_3 \tag{2.101}$$

where λ_3 is given in Figure 2.53.

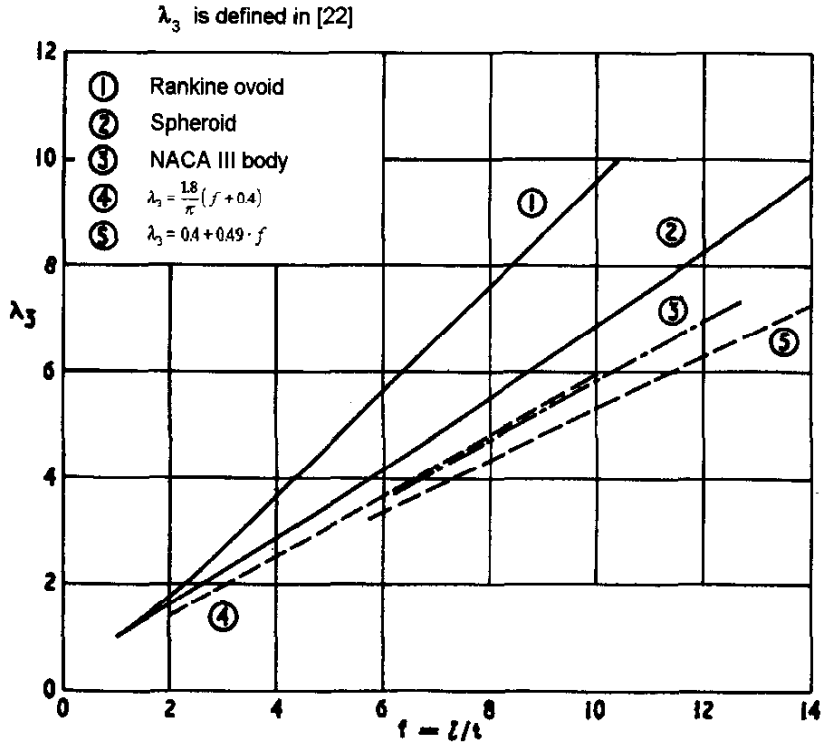

Figure 2.53 : Body-shape parameter

A more simple equation for circular open test sections in terms of Mach number, tunnel diameter and model volume is

$$\varepsilon_S = -0.0333\frac{V}{R^3}\cdot\frac{1}{\beta^3} \tag{2.102}$$

For the few tunnels with elliptical open test sections still in operation one may use the equation

$$\varepsilon_S = \left(T_R + 0.029\right)\left(\frac{1}{C}\right)^{3/2}\frac{V}{\beta^3} \tag{2.103}$$

where T_R can be taken from Figure 2.52 for a rectangular open jet with breadth/ height ratio equal to m/n and $C = \pi/4\, mn$.

2.4.4 WAKE CORRECTION

Little is known about wake blockage effects in open test sections; in most cases they are considered to be negligible. A sophisticated theoretical investigation is hardly worthwhile, since in any case the wake blockage effects will be disturbed by the wind tunnels individual collector inlet effects.

NOMENCLATURE FOR CHAPTER 2

A = effective cross-sectional area of 2D model = A_0 + added-mass area

A = rectangular tunnel aspect ratio = B/H

A_0 = dimensional cross-sectional area of 2D model

A_m = maximum transverse cross-section of model

a = body radius

B = tunnel breadth

C = cross-sectional area of test section

C_D = drag coefficient

C_d = drag coefficient for 2D model

C_L = lift coefficient

C_{LW} = lift coefficient of wing

C_l = lift coefficient for 2D model

C_M = pitching moment coefficient

C_p = pressure coefficient

c = airfoil chord

$\bar{c}$ = mean aerodynamic chord

d = distance of 2D vortex from the floor

f = body fineness ratio

H = tunnel height

K = nondimensional body shape factor; nondimensional factor for interference parameters; singularity strength

k = base pressure parameter

k = model span ratio $(\frac{Effective\ span}{Tunnel\ width})$

L = length; wing lift

M = Mach number

m = source strength

m = major axis of elliptical tunnel

n = spatial co-ordinate normal to the test section wall

n = minor axis of elliptical tunnel

p = static pressure

q = dynamic pressure

Re = Reynolds number

R_{max} = maximum body radius

r = cylindrical co-ordinate = $(y^2 + z^2)^{1/2}$

S = wing reference area

s = wing or vortex semi-span

s = source-sink separation distance for Rankine ovals and bodies

T = static temperature
t = maximum thickness
U = streamwise velocity
U_∞ = upstream reference velocity
u = perturbation x-velocity
$\boldsymbol{V}$ = total velocity vector = $\nabla\Phi$ for potential flow
V = velocity magnitude
V = effective model volume in 3D = V_0 + added-mass volume
V_0 = dimensional volume of 3D model
v = perturbation y-velocity
w = perturbation z-velocity
w_k = downwash correction at tail position
x = streamwise spatial co-ordinate
y = spanwise (or lateral) spatial co-ordinate
z = vertical spatial co-ordinate

Greek Symbols

α = angle of attack
β = Prandtl-Glauert compressibility factor = $(1 - M^2)^{1/2}$
γ = vortex strength in 2D = $1/2\ U_\infty\ c\ C_L$
Γ = vortex strength in 3D = $1/4\ U_\infty\ S\ C_L$
δ = lift interference parameter
δ_0 = lift interference parameter evaluated at the model centre
δ_ε = upwash interference due to blockage
δ_1 = streamwise curvature interference parameter
ε = blockage interference ratio = u_i / U_∞
ε_δ = streamwise interference due to lift
ζ = nondimensional vertical co-ordinate = z/L_{ref}
θ = blockage factor for bluff-body flow
Λ = wing sweep angle
λ = body shape factor
λ = test section height/width ratio
μ = doublet strength
η = nondimensional spanwise co-ordinate = y/L_{ref}
η = empirical factor for separated wake interference
ξ = nondimensional streamwise co-ordinate = $x/\beta L_{ref}$
ρ = fluid density
σ = nondimensional wing or vortex semi-span
τ = tunnel shape factor
Φ = total velocity potential

φ = perturbation potential

φ_m = perturbation potential due to the model

φ_w, φ_i = perturbation potential due to the walls (= interference potential)

Subscripts

b = base

c = corrected

corr = corrected

i = interference

m = model

n = normal

ref = reference

unc = uncorrected

w = walls

REFERENCES FOR CHAPTER 2

[1] AGARD, *Wind Tunnel Corrections for High Angle of Attack Models*, papers presented in Munich, Germany, May 1980, AGARD R-692, February 1981.

[2] AGARD, *Wall Interference in Wind Tunnels*, papers presented in London, UK, May 1982, AGARD CP-335, September 1982.

[3] Allen, H. J. and Vincenti, W. G., *Wall Interference in a Two-Dimensional-Flow Wind Tunnel with Consideration of the Effect of Compressibility*, NACA Report 782, 1944.

[4] Amonlirdviman, K., "Wind Tunnel Wall Interference Study Using A502 and Heyson's Wall Interference Code", unpublished analysis, August 1997.

[5] Ashley, H. and Landahl, M., *Aerodynamics of Wings and Bodies*, Addison-Wesley Publishing Co., 1965.

[6] Barnwell, R. W., "Similarity for Sidewall Boundary-Layer Effect in Two-Dimensional Wind Tunnels", *AIAA Journal*, Vol. 18, September 1980.

[7] Barnwell, R. W. and Sewall, W. G., "Similarity Rules for Effects of Sidewall Boundary Layer in Two-Dimensional Wind Tunnels", paper 3 in AGARD CP-335, 1982.

[8] Batchelor, G. K., "Interference on Wings, Bodies and Airscrews in a Closed Wind Tunnel of Octagonal Section", Report ACA-5 (Australia), 1944.

[9] Curtin, M. M., "DRA Wall Effects on High Lift Model", unpublished analysis, April 1994.

[10] Engineering Data Sciences Unit, "Upwash Interference for Wings in Solid-Liner Wind Tunnels Using Subsonic Linearised-Theory", ESDU 95014, October 1995.

[11] Fiddes, S. P. and Gaydon, J. H., "A Hybrid Panel/Image Method for Calculating Wall Constraint Effects in Subsonic Wind Tunnels", ICAS-94-3.3.2, 1994.

[12] Frink, N. T., "Computational Study of Wind-Tunnel Wall Effects in Flow Field around Delta Wings", AIAA 87-2420, August 1987.

[13] Garner, H. C., Rogers, E.W. E., Acum, W. E. A., and Maskell, E. C., "Subsonic Wind Tunnel Wall Corrections", AGARDograph 109, October 1966.

[14] GARTEUR Action Group AD (AG-02), "Two-Dimensional Transonic Testing Methods", GARTEUR TP-011, NLR TR 83086 U, July 1981.

[15] Glauert, H., "Wind Tunnel Interference on Wings, Bodies, and Airscrews", ARC R&M No. 1566, 1933.

[16] Goldstein, S., "Two-Dimensional Wind-Tunnel Interference", ARC R&M 1902, 1942.

[17] Havelock, T. H., "The Lift and Moment on a Flat Plate in a Stream of Finite Width", Proc. Roy. Soc., Series A, Vol. 166, 1938.

[18] Holst, H., "German Activities on Wind Tunnel Corrections," paper 4 in AGARD R-692, May 1980.

[19] Holt, D. R. and Hunt, B., "The Use of Panel Methods for the Evaluation of Subsonic Wall Interference", paper 2 in AGARD CP-335, September 1982.

[20] Joppa, R. G., *A Method of Calculating Wind Tunnel Interference Factors for Tunnels of Arbitrary Cross-Section*, NASA CR-845, July 1967.

[21] Joppa, R. G., *Wind Tunnel Interference Factors for High-Lift Wings in Closed Wind Tunnels*, NASA CR-2191, February 1973.

[22] Lock, C. N. H., "The Interference of a Wind Tunnel on a Symmetrical Body", ARC R&M 1275, 1929.

[23] Lynch, F. T., Crites, R. C., and Spaid, F. W., "The Crucial Role of Wall Interference, Support Interference, and Flow Field Measurements in the Development of Advanced Aircraft Configurations", paper 1 in AGARD CP-535, October, 1993.

[24] Magnus, A. E. and Epton, M. A., *PAN AIR - Computer Program for Predicting Subsonic or Supersonic Linear Potential Flow About Arbitrary Configurations Using a Higher Order Panel Method, Volume I, Theory Document (Version 1.0)*, NASA CR-3251, 1980.

[25] Maskell, E. C., "A Theory of the Blockage Effects on Bluff Bodies and Stalled Wings in a Closed Wind Tunnel", ARC R&M No. 3400, November 1963.

[26] Mokry, M., Chan, Y. Y., and Jones, D. J., edited by Ohman, L. H., "Two-Dimensional Wind Tunnel Wall Interference", AGARD AG-281, November, 1983.

[27] Murthy, A. V., *Corrections for Attached Sidewall Boundary-Layer Effects in Two-Dimensional Airfoil Testing*, NASA CR-3873, February, 1985.

[28] Murthy, A. V., *Effect of Aspect Ratio on Sidewall Boundary-Layer Influence in Two-Dimensional Airfoil Testing*, NASA CR-4008, September 1986.

[29] Murthy, A. V., *A Simplified Fourwall Interference Assessment Procedure for Airfoil Data Obtained in the Langley 0.3-Meter Transonic Cryogenic Tunnel*, NASA CR-4042, January, 1987.

[30] Murthy, A. V., "Correction for Aspect Ratio Effects in Airfoil Testing", DLR Report IB 222-90A15, March, 1990.

[31] Pope, A. and Harper, J. J., *Low-Speed Wind Tunnel Testing*, John Wiley & Sons, Inc., New York, 1966.

[32] Rueger, M. L., Crites, R. C., Weirich, R. F., Creasman, F., Agarwal, R. K., and Deese, J. E., "Transonic Wind Tunnel Boundary Interference Correction", paper 21 in AGARD CP-535, July 1994.

[33] Steinbach, D., *Calculation of wall and model support interferences in subsonic wind tunnel flows*, ZFW , Vol. 17, pp. 370-378, 1993.

[34] Theodorsen, T., *The Theory of Wind Tunnel Wall Interference*, NACA Report 410, 1931.

[35] Vaucheret, X. and Vayssaire, J. C., "Corrections de parois en écoulement tridimensionnel transsonique dans des veines a parois ventilées", paper 16 in *Wind Ttunnel Design and Testing Techniques*, AGARD CP-174, London, 1976.

[36] Vaucheret, X., "Améliorations des calculs des effets de parois dans les souffleries industrielles de l'ONERA", paper 11 in AGARD CP-335, May 1982.

[37] Wuest, W., „Verdrängungskorrekturen für rechteckige Windkanäle bei verschiedenen Strahlbegrenzungen und bei exzentrischer Lage des Modells." Z. Flugwiss, Vol. 9, pp 15-19 and Errata p. 362.